12-2017

Micro-Cantilever Based Fiber Optic Hydrophone

Jie Liu
Clemson University, jliu4@clemson.edu

MICRO-CANTILEVER BASED FIBER OPTIC HYDROPHONE

A Dissertation
Presented to
the Graduate School of
Clemson University

In Partial Fulfillment
of the Requirements for the Degree
Doctor of Philosophy
Electrical Engineering

---

by
Jie Liu
December 2017

Accepted by:
Hai Xiao, Committee Chair
Lin Zhu
John Ballato
Pingshan Wang

ABSTRACT

Endoscopic photoacoustic imaging probe is becoming increasingly important for many clinical photoacoustic imaging applications in which the target tissue can only be accessed by introducing an endoscopic probe percutaneously or through a natural orifice. Miniature fiber optic hydrophone (FOH) has become an attractive choice for endoscopic photoacoustic imaging application. Fiber optic hydrophone has many proven advantages, including small size, light weight, immunity to electromagnetic interference, low cost for single-use application and capability of integration of excitation light source and acoustic wave receiver.

This dissertation demonstrates an open cavity, micro-cantilever based fiber optic Fabry-Perot interferometer (FPI) hydrophone. A fused silica micro-cantilever beam as the sensing element is directly fabricated by femtosecond (fs) laser micromachining system. The theoretical analyses and experimental verifications were all applied for evaluation of the proposed cantilever based FOH.

A rectangular micro-cantilever based FOH is presented, which has a narrow bandwidth but high response and high sensitivity around its resonant frequency, and has many advantages as a good potential candidate for endoscopic photoacoustic imaging application. As a key parameter of the hydrophone, the resonant frequency can be adjusted by changing the dimensions and shapes of the micro-cantilever. In order to increase the resonant frequency of the rectangular micro-cantilever based FOH, and without loss in sensitivity, V-shaped and triangular cantilever based FOHs are investigated and compared with the rectangular cantilever based FOH theoretically and experimentally. The resonant

frequency of the triangular cantilever based FOH has been doubled without loss in sensitivity compared with the rectangular cantilever based FOH.

Cantilever based 45° angled FOH was proposed for a new choice for sideway looking detection except forward looking detection for endoscopic imaging in vessels. It consists of a fiber with a 45° angled endface and a fs laser fabricated micro-cantilever. The 45° angled endface would steer the optical axis by 90° via total internal reflection, and send the input light to the sensing part. This configuration could be applied for cross-axial sensing application. The proposed FOHs were all theoretically analyzed and experimental tested. Experimental results agree well with the simulated frequency responses of the proposed FOHs.

DEDICATION

This dissertation is dedicated to my dad, my family and friends, for their love, support and camaraderie.

ACKNOWLEDGMENTS

Foremost, I would like to express my sincere gratitude to my advisor Dr. Hai Xiao for his support of my Ph.D. study and research, for his patience and enthusiasm. His guidance helped me to finish the research, paper and writing of the dissertation. Without his support and encouragement, I couldn't finish my Ph.D. program. Again, thank him so much.

I am grateful to Dr. Lin Zhu, Dr. John Ballato, and Dr. Pingshan Wang, for serving on my dissertation comprehensive exam and defense, for their encouragements, valuable questions and suggestions.

I would like to express my acknowledgements to my labmates and friends I worked with in the Photonics Technologies Lab: Xinwei Lan, Jie Huang, Lei Yuan, Baokai Cheng, Wenge Zhu, Jincheng Lei and other members help me with the project.

I would also like to thank my husband Yuan Lei again for his support in my research and our family. Without his encouragement and support, I couldn't go through all difficulties and finish my Ph.D. program. I would like to thank my little boy, Leo Yuan who has made my life so meaningful and valuable.

TABLE OF CONTENTS

Page

Table of Contents (Continued)

Table of Contents (Continued)

LIST OF TABLES

LIST OF FIGURES

List of Figures (Continued) Page

List of Figures (Continued) Page

List of Figures (Continued) Page

LIST OF ACRONYMS

Fs/ps – Femtosecond/Picosecond Laser

SMF – Single Mode Fiber

MMF – Multimode Fiber

PVDF – Polyvinylidene Fluoride

OSA – Optical Spectrum Analyzer

SEM – Scanning Electron Microscope

FWHM – Full Width at Half Maximum

OPD – Optical Path Difference

MEMS – Micro-Electro-Mechanical Systems

FOH – Fiber Optic Hydrophone

GT – Glass Tube

FP - Fabry-Perot

EFPI – Extrinsic Fabry-Perot Interferometer

FPI – Extrinsic Fabry-Perot Interferometer

FIB – Focused Ion Beam

FBG – Fiber Bragg Grating

EMI – Electromagnetic Interference

SNR – Signal Noise Ratio

CHAPTER ONE

INTRODUCTION

1.1 HYDROPHONES

Titanic's sinking stunned the world, and captured the world's attention in April, 1912. Within two months of the disaster, Reginald Fessenden patented a high-frequency oscillator, and then he worked out the earliest used hydrophone to detect an iceberg 2 miles away. It was an electro-acoustic transducer and a first successful acoustical echo ranging device in 1917 [1]. During the World War I, Langevin and his group utilized the dual nature of the piezoelectric effect of quartz crystal to realize a piezoelectric hydrophone device for defensing the Germen submarines' attack [2-3]. Piezoelectric hydrophone are the most common devices used for acoustic measurements in water. The industrial and military applications of ultrasound detection were lead to the development of medical diagnostic ultrasound technology.

Nowadays, hydrophones are used in a variety of applications, such as ocean observation, environmental monitoring, pile driving, oil/gas pipeline leak detection and biomedical photoacoustic imaging. Researchers proposed the feasibility of ultrasound generation by irradiation of a solid with a laser pulse in early 1960s, during next twenty years, the elastic wave generated by the interaction of a laser pulse with a solid had been published in many literatures [4]. Afterwards, the optical ultrasound detection and imaging have made greatly progress. Miniature size, highly sensitive hydrophones are useful for endoscopic photoacoustic imaging in which the optically excited broadband and low amplitude ultrasonic waves are detected by one or more hydrophones and used to construct

the tomography of optically contrasted functions and properties of tissues and organs [5-9].

The earliest fiber optic hydrophone (FOH) was based on phase modulation, applied acoustic-optic interaction directly on optical fiber in 1977 [10]. FOHs have attracted much attention and been researched for decades. Alternative approaches include intensity modulation, frequency or wavelength modulation and phase modulation [11-14]. Fiber optic systems have telemetry over long distance without additional power compared with other electroacoustic systems [15]. By taking advantage of optical fiber, FOH have the unique advantages, including small size, immunity to electromagnetic interference (EMI), low cost and the unique capability to integrate the excitation light source with acoustic receiver for clinical endoscopic photoacoustic imaging application [16-19]. The most common design of FOH is diaphragm based fiber optic Fabry-Perot interferometric (FPI) hydrophone. The FPI structure has a very small sensing area and is particularly attractive for endoscopic photoacoustic imaging. Various diaphragm based extrinsic Fabry-Perot interferometer (EFPI) FOH have been reported [20-29]. In our previous work, silica diaphragm based EFPI acoustic sensor has been proposed as well [30].

1.1.1 PVDF hydrophone

Piezoelectric effective is defined as the linear electromechanical interaction between the electrical charges and stress distribution in piezoelectric material. Piezoelectric transducers have been widely used for ultrasonic medical imaging and photoacoustic imaging [31-32]. Piezoelectric hydrophone is an active hydrophone, which is known as

pulse-echo mode. It is because piezoelectric hydrophone is based on piezoelectric effect, which can be used for exciter and receiver. Flexible piezoelectric polymers, most notably Polyvinylidene Fluoride (PVDF), have been commonly used for construction of small size acoustic imaging devices. The size of commercial PVDF hydrophone could go down to ten millimeters in diameter, however, the element size is difficult below 0.5 mm due to 'fringe' effects involved with spot poling PVDF films [33]. PVDF has low permittivity, high mechanical losses and low piezoelectric constants. PVDF hydrophones usually need complex designs and multiple impedance matching layers to reach the performance of the piezoelectric ceramic hydrophones [34-35].

1.1.2 Fiber optic hydrophones

FOHs have also been used for photoacoustic imaging [36-40]. Compared with the piezoelectric hydrophones, FOHs have the unique advantages, including small size, flexibility and the capability to be integrated with the excitation light source, which make them particularly attractive for endoscopic imaging. In addition, because of their immunity to EMI, FOHs can be used in a strong EMI and electric shocking hazardous environment such as in an electric transformer [41]. Various fiber sensors have been investigated for acoustic wave detection underwater. These sensors operate by detecting the acoustic pressure induced different optical parameters such as intensity [42-45], frequency and wavelength [46-50], and phase [51-54].

1.1.2.1 Intensity modulation FOHs. Intensity-based FOHs are easy to fabricate and integrate. By monitoring reflection or transmission loss, vibration of the free end of

the optical fiber caused by acoustic wave could be detected and analyzed [42-45]. However, their sensitivities are found to be inadequate. Arnaud et al. presented an intensity based optic probe hydrophone utilizing refractive index changed by cavitation in water that results from acoustic wave [42].

1.1.2.2 Wavelength modulation FOHs. A fiber Bragg grating (FBG) is that reflective elements written into the core of an optical fiber, its specific wavelength, also called Bragg wavelength would be reflected and the others would transmit. The Bragg wavelength could be changed when grating period changed. The mechanism of FBG hydrophone is based on wavelength modulation. Takahashi et al. proposed an underwater acoustic sensor using FBG in 1997 [47]. Baiou Guan's group presented a distributed Bragg Reflector Fiber laser used as ultrasonic hydrophone [50]. Shuaiqi Jing et al. applied FBG for photoacoustic imaging in 2015 [49]. However, the upper limit of the incident acoustic frequency is set by the length of the grating.

1.1.2.3 Interferometric modulation FOHs. The literature on optical fiber interferometric acoustic sensor is extensive. The earliest FOH was realized with fiber optic interferometer. Optical fiber interferometers are preferred to construct the hydrophone when a detection sensitivity is needed. Mechanism of interferometric hydrophone include Mach-Zehnder [52], Fabry-Perot [51], Michelson [55], Sagnac [56] and ring resonator [57-59].

Among the many demonstrated optical fiber interferometer based hydrophones, the FPI based structure has a very small sensing area and is particularly attractive for endoscopic photoacoustic imaging. A typical fiber optic EFPI hydrophone uses a thin

diaphragm as the sensing element, which deflects under the acoustic pressure to produce a change in the optical path difference (OPD). The change in OPD is measured by the interferometer with a very high sensitivity and at a high speed. The diaphragm can be made of various materials, such as metal, polymer, fused silica and etc.

However, a soft diaphragm will result in a high sensitivity but low frequency response. The other considerations in choosing the diaphragm material include temperature cross sensitivity, mechanical robustness and acoustic impedance matching. Both sealed and open cavity FPI sensors have been reported for acoustic wave measurement [20]. In general, a sealed cavity sensor has a wide and relatively flat frequency response (all the way from static pressure) while the open cavity sensor has a higher sensitivity but limited acoustic detection bandwidth. The sealed cavity sensor will also face the problem of operating point drift due to temperature variations of static pressure changes.

The traditional way of making the fiber optic FPI hydrophone is to assemble the diaphragm with the optical fiber to make the FPI structure. However, assembly-based sensors have difficulty to precisely control the initial cavity length as well as other issues such as operating point drift and weak mechanical robustness. More recently, various micromachining techniques have been used to directly fabricate fiber FPI sensors. These assembly-free sensors have shown advantages of high dimensional precision, compactness, improved sensitivity and mechanical strength. In this dissertation, we report compact cantilever-based open cavity fiber optic FPI hydrophones fabricated by femtosecond laser (fs) micromachining.

1.1.2.4 Fiber sensor with a 45° angled endface. Fiber optic sensors utilized total internal reflection at the 45° angled fiber endface to steer the optical axis by 90 ° to achieve more optional sensing application on the sidewall of the optical fiber. There are several kinds of angled fiber optic sensors applied for pressure sensing [60] and temperature sensing [61-63]. 45 ° angled endface provides a good choice for cross-axial sensing.

1.2 Micromachining methods for micro-cantilever beam

Micro-machined cantilevers are widely used for atomic force microscopy, chemical/biological detection and physical parameters monitoring. These applications are all based on measuring the mechanical deformation of the cantilever in response to certain external events. Micro-cantilever is small, robust, does not need alignment and can potentially operate in harsh environment. Nowadays, several methods have been reported to fabricate micro-cantilever structure including MEMS [64], Picosecond (Ps) laser [65], Focused Ion Beam (FIB) [66-67], and fs laser [68]. Fs laser micromachining has been a promising method for fabrication of micro/Nano-structures in/on optical fiber tips attributed to its high precision, flexible design, assembly free, and compatible with other methods such as sputter coating, and fusion splicing [69].

1.3 Motivations and objectives

Motivations: This research was initially motivated by developing a novel micro-cantilever based FOH with help of fs laser micromachining system for clinical endoscopic photoacoustic imaging. The assessment of coronary artery disease, prostate cancer and

gastrointestinal pathologies needs high sensitivity, miniature size, flexible and low cost for single-use endoscopic imaging probes [16]. Small fiber optic imaging probe could be used in photoacoustic imaging system for guiding minimally invasive procedures for visualizing tissue structures such as blood vessels, nerves and tumors and needle tracking [70-71], the noncontact measurement of the photoacoustic tomography [37], 3D photoacoustic imaging of blood vessel phantoms [39], and high resolution vascular tissue imaging [40] in ultrasound bandwidth of ~20MHz.

The micro-cantilever based FOH offers flexibility in configuration for forward looking detection and sideway looking detection by changing the sensing part location. It still has capability to integrate the transmission of light and acoustic wave receiver. The motivation of the research is to meet the requirements of developing an endoscopic photoacoustic imaging probe for clinical applications.

Objectives: From the previous reviews, EFPI is a good choice for fiber optic sensing application. A fused silica micro-cantilever could be realized easily by using fs laser micromachining system. Integrating EFPI and fs laser fabricated fused silica micro-cantilever into a micro-cantilever based FOH to achieve a miniature, inexpensive, assembly free, sensitive to acoustic wave endoscopic probe. The main objective of the research is realizing the concept of the micro-cantilever based FOH, we will be focusing on design, model, fabrication and test the proposed micro-cantilever based FOH. The specific objectives of this research include:

1) Deep understanding the behavior of immersed micro-cantilever beam, model and numerical simulation the dynamic response of the sensing micro-cantilever beam.
2) Optimization of the rectangular cantilever based FOH for predesign of the resonant frequency of the hydrophone.
3) Development of the ultrafast laser micromachining system for micro-cantilever based FOH fabrication.
4) Design and implement a measurement system including both optical and RF devices to evaluate the dynamic response of the proposed hydrophones.
5) Characterize the hydrophone with items of dynamic response, sensitivity, detection limit experimentally.

1.4 Organizations of the dissertation

This dissertation is organized into six chapters with its contents summarized below:

Chapter 1 introduces the history and development of hydrophones. Started with an oscillator used for iceberg detection, piezoelectric materials have been used for underwater acoustic transducers for nearly a century. Piezoelectric polymers are often used for small size hydrophones because of its flexibility and acoustic impedance matching with water, especially PVDF. FOH have been researched for decades benefited from unique properties of optical fibers. For photoacoustic imaging application, diaphragm based FOHs have attracted much attentions. A brief review of FOHs is provided.

Chapter 2 describes the principles of EFPI. The theory of the micro cantilever beam is derived, not only for rectangular cantilever but also V-shaped and triangular cantilever beams. Finite element analysis with COMSOL is described in details. After that, the mechanism of the proposed hydrophone is expressed.

Chapter 3 describes the fabrication of recantangular cantilever based FOH. Acoustic wave measurements in air and under water are all presented.

Chapter 4 introduces V-shaped and triangular cantilever based FOHs. The fabrication, optimization and predesign of the different shaped micro-cantilever based FOHs. Dynamic responses of the hydrophones were experimentally tested and theoretically analyzed.

Chapter 5 describes sideway looking detection hydrophone that is cantilever based 45 ° angled FOH. The different fabrication is described in details. This sideways looking hydrophone is characterized with its dynamic response, sensitivity. The advantages of the hydrophones will be discussed.

Chapter 6 summarizes the dissertation work and comments the future work.

1.5 Innovations and contributions

Scientific and technical contributions of the research include the following:

1. A novel, open cavity, micro-cantilever based FOH was proposed and realized with help of fs laser precise micromachining system. Experimental analysis demonstrated dynamic response of the hydrophone, and were in good agreement with theoretical investigations and numerical simulation results.

2. The use of V-shaped and triangular cantilever beams for atomic force microscope inspired the sensing structure design. By changing the shapes of the sensing part of the hydrophone from rectangular cantilever to V-shaped or triangular cantilever, the resonant frequency of the hydrophone could be predesigned and doubled without loss in sensitivity.
3. Cantilever based 45° angled FOH was realized for cross-axial sensing by directing the input light sideways in using total internal reflection on the angled endface. The micro-cantilever as sensing structure had much more space in design. This hydrophone provided an approach in sideways looking detection, which is meaningful for endoscopic application.

CHAPTER TWO

THE MECHANISM OF THE MICRO-CANTILEVER BASED FOH

This chapter will introduce the operating principles of the micro-cantilever based FOH, which is based on EFPI. The principles of EFPI will be described firstly. The sensing part of the FOH is a micro-cantilever beam. The properties and behavior of the immersed micro-cantilever will be investigated and described. Finite element analysis is conducted with COMSOL to explore the dynamic response of the immersed complex geometrical structures.

2.1 Principles of EFPI

The representative diaphragm based EFPI sensor is shown in Fig. 2.1. Light goes through the lead-in fiber, and is reflected by the two mirrors, which are the interface between the lead-in fiber and the EFPI cavity, and the inner endface of the diaphragm, forms a typical interference signal.

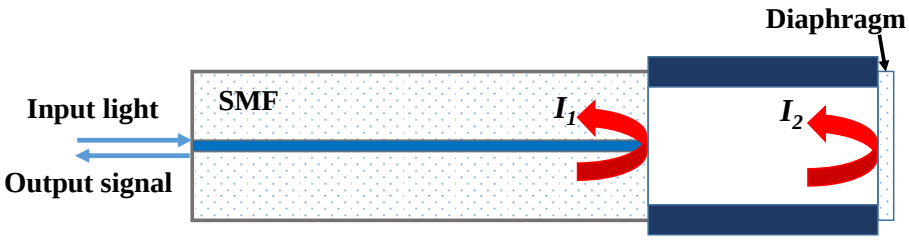

Fig. 2.1. Schematic of a diaphragm based EFPI sensor.

This EFPI sensor could be modeled using the classical two-beam interference equation

$$I = I_1 + I_2 + 2\sqrt{I_1 I_2}\cos(\frac{4\pi n_0 L}{\lambda} + \varphi_0) \tag{2.1}$$

where I is the intensity of the interference signal, I_1 and I_2 are reflected signals from those two different interfaces, n_0 is the refractive index of the medium filled in the cavity of the EFPI, L is the cavity length, *and* φ_0 is the initial phase of the interference.

The intensity of the interference signal reaches its valleys periodically when the phase of the cosine term in Eq. (2.1) becomes an odd number of π. The phase difference between the adjacent dips is 2π. The adjacent dips are supposed to be at λ_1 and λ_2, the phase difference could be express as

$$\frac{4\pi n_0}{\lambda_1} L - \frac{4\pi n_0}{\lambda_2} L = 2\pi \tag{2.2}$$

Thus, the cavity length L will be obtained from Eq. (2.3), that is

$$L = \frac{\lambda_1 \lambda_2}{2n_0 \left(\lambda_2 - \lambda_1\right)} \tag{2.3}$$

where λ_1 and λ_2 are the center wavelength of the adjacent dips.

2.2 Theory of immersed micro-cantilever

2.2.1 Rectangular micro-cantilever

When the micro-cantilever beam was immersed in water and excited by an acoustic wave, the dynamic deflection of the cantilever beam can be modeled and analyzed using the general theory given in Ref [72] which described the dynamic response of a cantilever beam under a point load for atomic force microscope applications. Here we adopt it to study the frequency response of the cantilever under the distributed acoustic load.

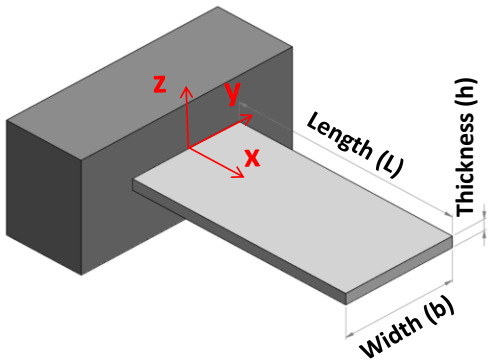

Fig. 2.2. The structure and dimension of the rectangular cantilever beam with uniform cross-section.

Figure 2.2 shows the schematic of a cantilever for the purpose of analyses. The length, width and thickness are *L*, *b* and *h*, respectively. The deflection *w(x, t)* of the cantilever beam is given by

$$EI\frac{\partial^4 w(x,t)}{\partial x^4}+\mu\frac{\partial^2 w(x,t)}{\partial t^2}=F(x,t) \tag{2.4}$$

where *E* is Young's modulus; *I* is the moment of inertial of the cross section of the beam; μ is the mass per unit length of the beam; *F(x, t)* is the external force function loaded on the cantilever beam; *t* is the time variable. The spatial variable *x* varies along the length of the cantilever beam.

For the micro-cantilever structure, the boundary conditions include four parts: (1) the fixed end of the beam doesn't have any deflection; (2) the derivative of the deflection at the fixed end is also zero; (3) there is no bending moment at the free end of the cantilever, so the second order derivative at the free end is zero; (4) there is no shearing force acting at the free end of the beam, thus the third order derivative is still zero.

In order to obtain the deflection function in the frequency domain the Fourier transform is applied to Eq. (2.4), which produces

$$\frac{EI}{L^4}\frac{d^4\hat{W}(x,\omega)}{dx^4} - \mu\omega^2\hat{W}(x,\omega) = \hat{F}(x,\omega) \tag{2.5}$$

Typically, the external force needs to be separated into two components

$$\hat{F}(x,\omega) = \hat{F}_{hydro}(x,\omega) + \hat{F}_{drive}(x,\omega) \tag{2.6}$$

where $\hat{F}_{drive}(x,\omega)$ is the applied driving force. If we assume the acoustic wave has a single frequency and uniformly exerts a force onto the beam at the direction perpendicular to the beam, $\hat{F}_{drive}(x,\omega) = A$ where A is the amplitude of the driving force. $\hat{F}_{hydro}(x,\omega)$ is the hydrodynamic loading force caused by the motion of the fluid around the beam, given by

$$\hat{F}_{hydro}(x,\omega) = \frac{\pi}{4}\rho\omega^2 b^2\Gamma(\omega)\hat{W}(x,\omega) \tag{2.7}$$

where ρ is the density of the fluid and $\Gamma(\omega)$ is defined as the hydrodynamic function per Ref [72]. Therefore, Eq. (2.5) can be written as

$$\frac{d^4\hat{W}(x,\omega)}{dx^4} - \frac{\mu\omega^2 L^4}{EI}\left(1+\frac{\pi\rho b^2}{4\mu}\Gamma(\omega)\right)\hat{W}(x,\omega) = \frac{AL^4}{EI} \tag{2.8}$$

The Green's function theory is used to solve Eq. (2.8) by applying the boundary conditions. The deflection $\hat{W}(x,\omega)$ is found to be

$$\hat{W}(x,\omega) = \int_0^L G\left(x,x'|w\right)\frac{AL^4}{EI}dx' \tag{2.9}$$

The expression of the Green's function can be found in Ref. [25].

It is well known that the dimensions and physical properties of a micro-cantilever strongly affect its dynamic response, and the frequency response of the micro-cantilever is also strongly depending on the fluid in which it is immersed [72-73]. So it is highly

desirable to involve numerical simulations to figure out the relationship between the different dimensions of a micro-cantilever beam and the frequency responses. The numerical simulation results are presented and analyzed as follows.

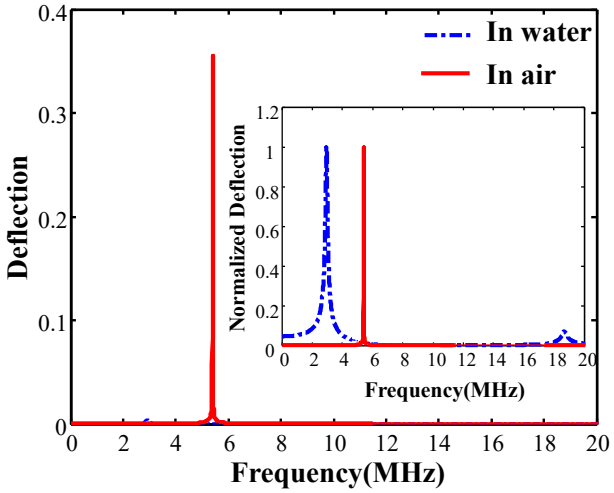

Fig. 2.3. Deflection spectra of the cantilever-based fiber optic sensor immersed in fluid, the dashed blue line shows the spectrum in water, and solid red line presents the spectrum in air. Inset: Normalized deflection spectra of the cantilever-based fiber optic sensor immersed in fluid with respect to their highest response.

In the simulated frequency response spectra of the cantilever based optical fiber acoustic sensor shown in Fig. 2.3. The effective length, width and thickness of the micro-cantilever part are 80 μm, 50 μm and 15 μm respectively. Due to the material of micro-cantilever is fused silica, the young's modulus is 73 GPa, and the Poisson's ratio is 0.17. The viscosity coefficients of water and air are 2.5e-3 and 1e-5 Pa·s, respectively. The frequency response spectra in fluid are all calculated by using Eq. (2.9).

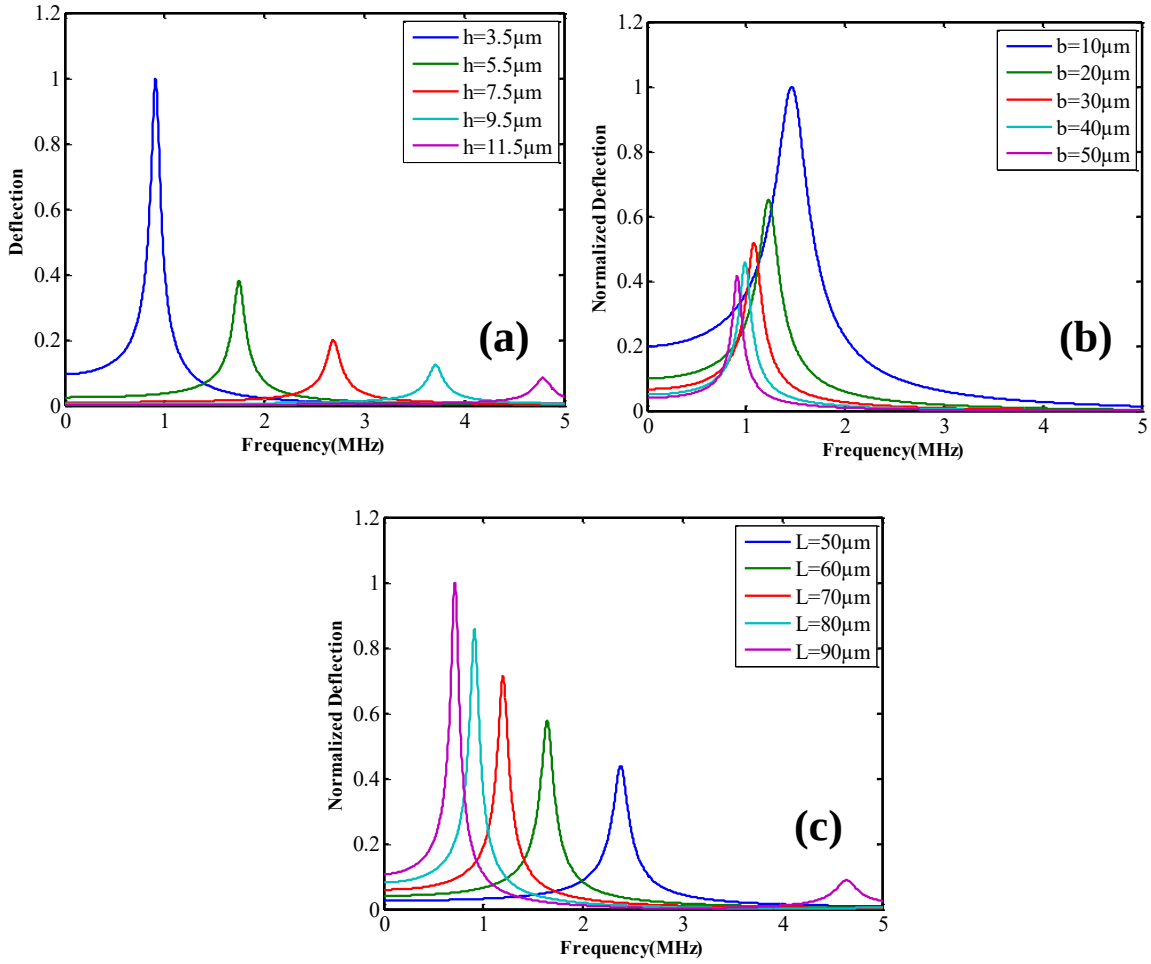

Fig. 2.4. Normalized deflection spectra of the micro-cantilever immersed in water in different dimensions with respect to the highest response. (a) The width of cantilever was 45 μm, and the length was 85 μm. (b) The thickness and the length of cantilever were 9 μm and 85 μm respectively. (c) The width of cantilever is 30 μm, the thickness was 9 μm.

The fundamental frequency of the micro-cantilever in air is 5.4 MHz as shown in the red solid line in Fig. 2.3. The frequency response of the micro-cantilever in water is dashed blue line in Fig. 2.3, which is much weaker than the dynamic response in air. For better comparison, we normalized the frequency response spectra with respect to their

highest deflection as shown in the inset of Fig. 2.3. The fundamental frequency of the micro-cantilever in water is 2.9 MHz, and the fundamental frequency and first harmonic frequency are all clear as shown in dashed blue line of the inset of the Fig. 2.3. It is much clear that the fundamental frequency in water is much smaller than it in air, and also is broadened because the different viscosities of the fluid around the cantilever.

Length, thickness and width are three main parameters for designing the rectangular micro-cantilever beam. By changing one of these three parameters in calculations, we can find the relationship between the dimensions and the frequency spectra. The results in Fig. 2.4(a), demonstrate that for given width and length of the micro-cantilever structure of 45 μm and 85 μm, respectively, an increase in the thickness of the micro-cantilever over range from 3 μm to 15 μm has the effect of weakening and increasing the resonance peak to higher frequencies. In Fig. 2.4 (b), we use the conformed thickness and length, 9 μm and 85 μm, and change width of the micro-cantilever from 10 μm to 50 μm to get the shifting resonance frequencies in different response spectra. In Fig. 2.4(c), the thickness and the width are given as 9 μm and 30 μm, it is clearly showed that sweeping the length in range from 55 μm to 95 μm has improved the deflection of the fundamental frequencies and shifted the resonance peak to lower frequencies. The relationship between the size of the cantilever and the dynamic response is clear. Increasing thickness will lift the fundamental frequency obviously. However, the changes of thickness still bring amounts of changes to the deflection. The wider the width of micro-cantilever is, the lower the fundamental frequency will be. Improving the length of the cantilever structure will reduce the

fundamental frequency and improve the deflection. Among the three dimensions of the micro-cantilever, thickness is the dominant parameter to effect the frequency response.

2.2.2 V-shaped and Triangular cantilever

V-shaped micro-cantilever is currently popular in the applications of the atomic force microscope (AFM). The use of V-shaped cantilever is due to its insensitivity to lateral twisting and rolling, even it is still in dispute [74]. Theoretical investigation of the spring constants of the rectangular and V-shaped cantilevers have been reported in literature [75]. The spring constant of the V-shaped cantilever is equivalent to it of the rectangular cantilever which has same length and thickness but twice the width of the one arm of the V-shaped cantilever [75-76], which make the resonant frequency of the V-shaped cantilever can be improved a lot compared with rectangular cantilever but almost no loss of sensitivity. Triangular cantilever emphasizes resonant frequency improvement than V-shaped cantilever, and is easier in micro-fabrication. Fig. 2.5 shows shapes and dimensions of the two different cantilever structures. The spring constants could be estimated using Eqs. (2.10) and (2.11) based on the dimensions shown in Fig. 2.5.

The spring constant of an end-loaded rectangular cantilever beam is given by

$$k = \frac{Et^3 w}{4L^3} \tag{2.10}$$

where w is the width, L is the length, and t is the thickness, E is the elastic modulus.

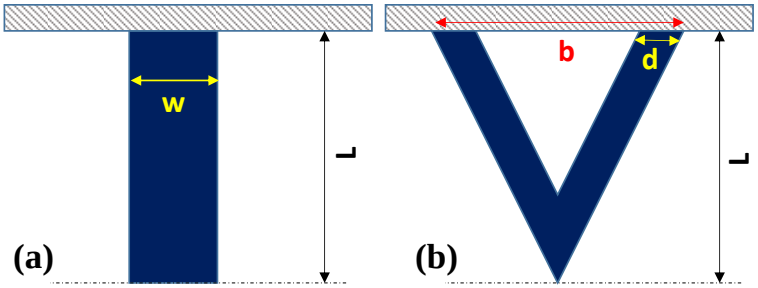

Fig. 2.5. Shape and dimensions of (a) rectangular cantilever (b) V-shaped cantilever.

Due to the symmetry of the V-shaped cantilever, the parallel beam approximation is applied in analytical evaluation of the spring constant of V-shaped cantilever beams, which is effective and simple [75]. The zeroth order spring constant solution was obtained

$$k = \frac{Et^3 d}{2L^3}\left\{1+\frac{4d^3}{b^3}\right\}^{-1} \tag{2.11}$$

For V-shaped and triangular cantilevers, it is difficult to get the vibration responses from formulas in immersion case. However, as a part of the resonant sensor, the resonant frequency is an important parameter. The static resonant frequencies of the V-shaped cantilever are explored in many literatures [77-79]. The Rayleigh-Ritz method is often used in mechanical engineering to estimate the approximate real resonant frequencies of multi degree of freedom systems. Thus, the Rayleigh-Ritz method provides the approach to calculate the resonant frequencies of V-shaped and triangular cantilevers, which helps the researchers in designing and optimization of V-shaped and triangular cantilevers.

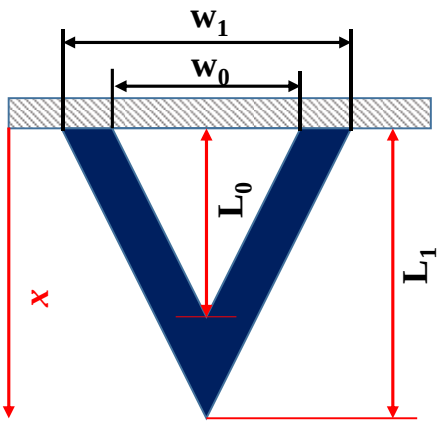

Fig. 2.6. Shape and dimensions of V-shaped cantilever.

The resonant frequency of a cantilever with an arbitrary shape but uniform thickness can be obtained using Rayleigh-Ritz method as

$$f(W(x)) = \frac{t}{2\pi}\sqrt{\frac{3E}{\rho}}\sqrt{\frac{\int_0^L W(x)(L-x)^2 dx}{\int_0^L W(x)x^4(3L-x)^2 dx}} \tag{2.12}$$

where *W(x)* is the width function, L is the length of the cantilever, ρ is density of the structure. Figure 2.6 shows a typical symmetrical V-shaped cantilever, obviously, the width function can be simplified as

$$W(x) = \begin{cases} \frac{W_1}{2}(1-\frac{x}{L_1}) - \frac{W_0}{2}(1-\frac{x}{L_0}), x \in [0, L_0] \\ \frac{W_1}{2}(1-\frac{x}{L_1}), x \in [L_0, L_1] \end{cases} \tag{2.13}$$

From Eqs. (2.12) and (2.13), triangular cantilever can reach the maximum resonant frequency and highest sensitivity. The frequency is obtained

$$f = \frac{t}{2\pi L_1^2}\sqrt{\frac{70E}{\rho}}\frac{\sqrt{3}}{7} \tag{2.14}$$

Static resonant frequencies of V-shaped cantilever and triangular cantilevers are all presented and discussed, which are very helpful for predesign. However, the dynamic responses of the immersion V-shaped and triangle cantilevers need more powerful tool's help.

2.3 Finite element analysis

Finite element analysis was conducted with commercial software COMSOL, which help us to analyze the dynamic response of the immersed complex geometrical structures effectively and economically.

When the cantilever beams are immersed in a fluid, the fluid affects the mode shapes of immersed cantilever beams, and damping will reduce their fundamental frequencies. However, the phenomenon is difficult to be expressed in formulas. In the simulation, a Multiphysics approach is chose to find out fundamental frequencies and mode shapes of the immersed cantilever beams. The problem is set up as a coupled acoustic-structure eigenvalue analysis. Fluid viscosity is added as a viscous loss term for damping. Due to the scale of the micro-cantilever, the surrounding fluid geometric block are ten times sizes of the cantilever structure. The fluid space has sound hard boundary, and the COMSOL automatically defines the interfaces between cantilever structure and the fluid.

The parameters used in simulation are listed in table 2.1. The bulk viscosity needs to be added from viscosity model. The value of bulk viscosity of water is from the Ref. [80].

Table 2.1 COMSOL simulation parameters

Material	Properties	Values	Unit
Water	Density	997	kg/m^3
	Speed of sound	1450	m/s
	Bulk viscosity	2.5e-3	Pa·s
Silica glass	Density	2203	kg/m3
	Young's modulus	73e9	Pa
	Poisson's ratio	0.17	_

Figure 2.7 shows the immersion V-shaped cantilever model, one end of the cantilever beam is added fixed constraint, while the tip end is free. Eigen-frequency study is applied to explore the first mode frequency of the immersed cantilever beam.

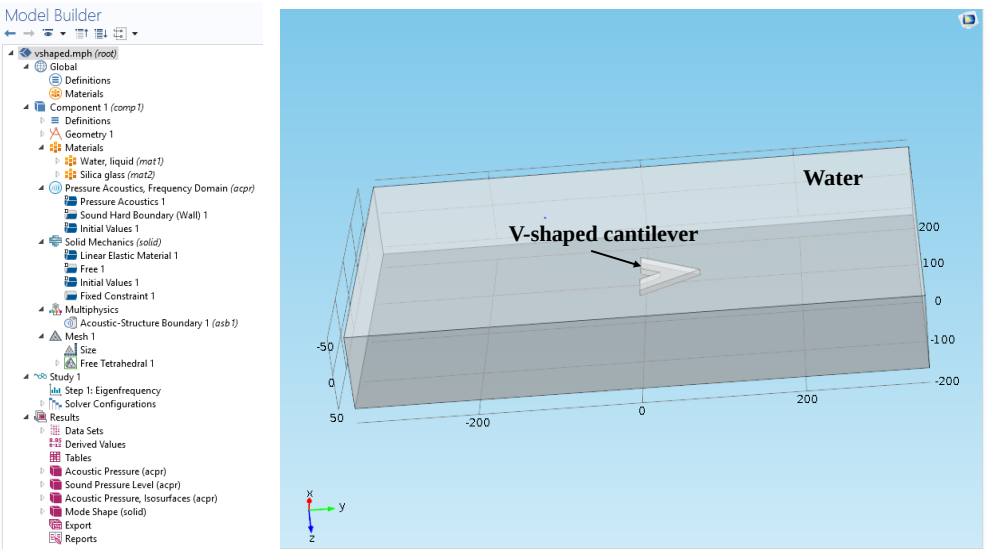

Fig. 2.7. The immersed V-shaped cantilever model.

The mode shape is shown in Fig. 2.8, from mode shape, the resonant frequency can be distinguished easily. Resonant frequencies of the modes of the cantilever beam vibrating

in fluid environment are calculated via Eigen frequency solver. The complex cantilever structure is analyzed effectively with the help of COMSOL.

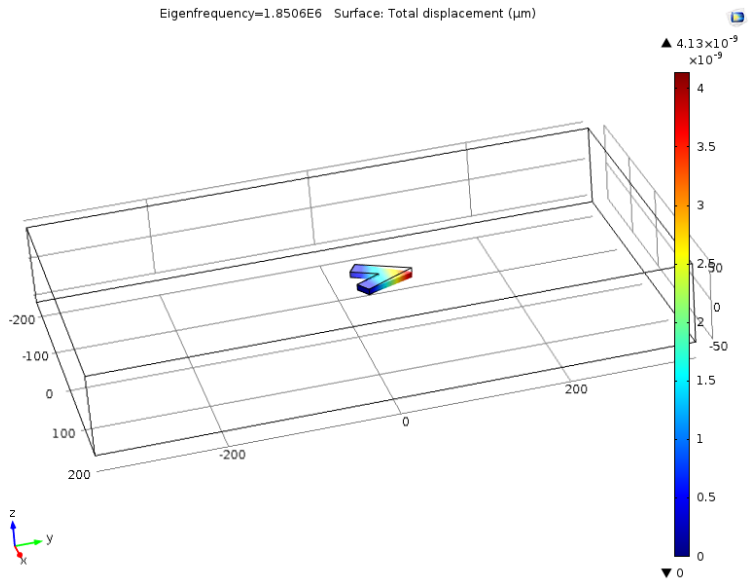

Fig. 2.8. Mode shape of the immersed V-shaped cantilever model.

To assess the correctness of the model we used and the accuracy of the results, we used rectangular cantilever to compare two simulation results, one is from COMSOL shown in Fig. 2.9 and the other is numerical simulation from Eq. (2.9). Those two simulations used same dimensions and same properties. The first mode frequency is 0.72 MHz in numerical simulation, and the COMSOL shows the first mode frequency is 0.84 MHz. Two simulation results has a very good agreement. This modeling would help a lot in predesigning the resonant frequency of the micro V-shaped and triangle cantilever based FOHs.

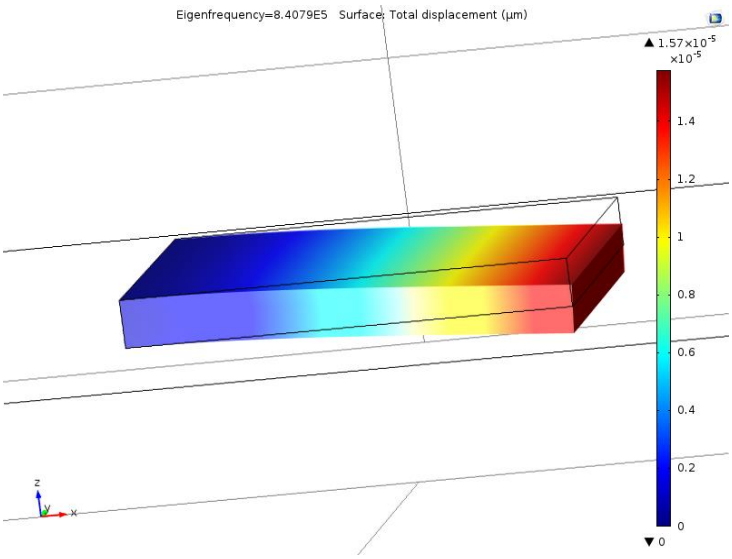

Fig. 2.9. The first Mode shape of the immersed rectangular cantilever model.

2.4 Principles of micro-cantilever based FOH

Combine EFPI and micro-cantilever theory, with the help of micromachining technology, the micro-cantilever based FOH is proposed.

Figure 2.10 illustrates the structure and operating principle of the cantilever based FOH. The single mode fiber (SMF), glass tube (GT) and the micro-cantilever form an open Fabry-Perot (FP) cavity. The outer surface of the micro-cantilever is laser roughened during the fabrication process. Thus, the FPI has only two reflections at the fiber endface (I_1) and the inner surface of the cantilever (I_2), respectively. These two reflections superimpose to generate an interference signal when excited by a laser source. The impinging acoustic waves make the micro-cantilever vibrate and correspondingly change the OPD of the FP cavity, resulting in the change in optical intensity around the biasing point (also referred to as the operating point). Typically, the operating point is chosen in

the center region of the sinusoidal interference signal to achieve a linear response with high sensitivity.

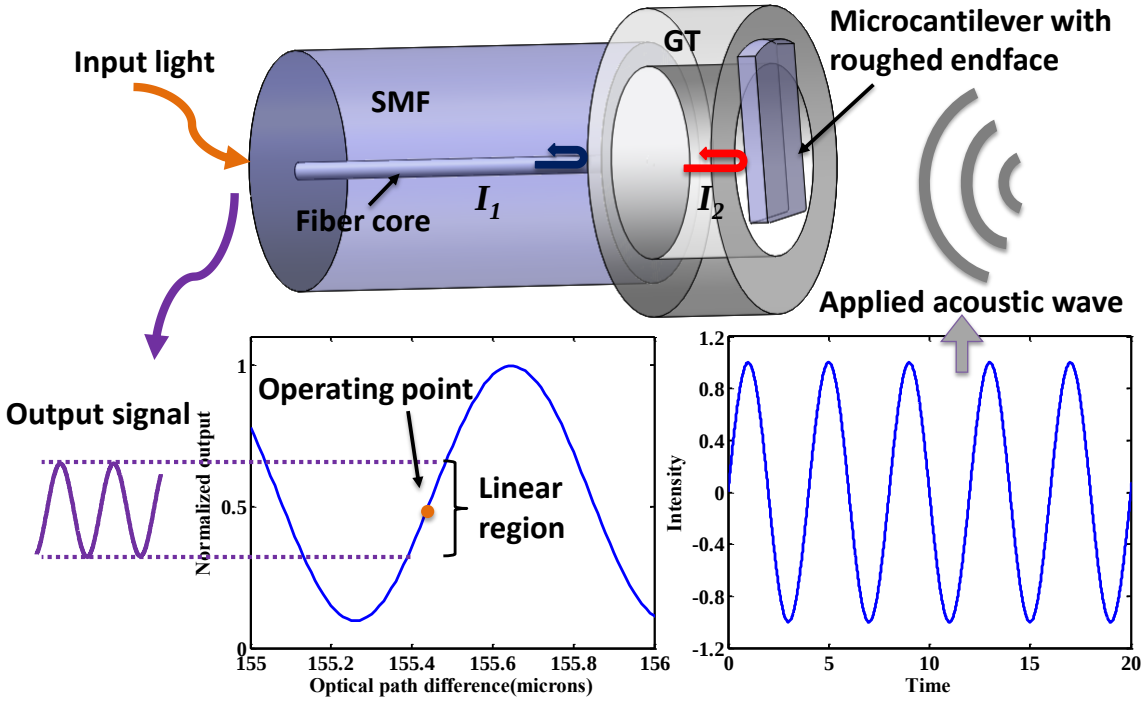

Fig. 2.10. Structure and operating principle of the micro-cantilever based FOH.

CHAPTER THREE

RECTANGULAR CANTILEVER BASED FOH

We report an open cavity, rectangular cantilever based fiber optic FPI hydrophone in this chapter. The hydrophone is made of fused silica material, and its micro-cantilever beam is directly fabricated by femtosecond (fs) laser micromachining. The theoretical analysis and experimental verification of the frequency response of the sensor are presented.

3.1 Hydrophone fabrication

3.1.1 Sample preparation

Typically, sensor fabrication consists of the following steps: First, an FP interferometer was fabricated at the tip of an SMF. A section of a capillary GT with an outer diameter of 170 μm and an inner diameter of 100 μm (TSP100170, Polymicro, Inc.) was initially spliced to a standard single-mode fiber. Then, the tube was cleaved at a distance (tens of micrometers) from the splice point with the help of a microscope. The tube was then spliced to another SMF to form a sealed air cavity sandwiched between two fibers. The whole parts could be regarded as a SMF-GT-SMF structure. Precision fiber cleaving was applied to cut the fiber so that a thin piece of fiber was left to perform as a diaphragm. Finally, the as-cleaved diaphragm was thinned and fabricated to a thin diaphragm followed by a cantilever structure by using an fs laser [81].

3.1.2 Development of fs laser micromachining system

Recent progress in the fs laser three-dimensional (3D) micro- and even Nano-scale micromachining technique offers an effective and flexible way for high precision fabrication of microdevices and structures in various transparent materials, such as fused silica glass [82-85] and crystal sapphire materials [86]. When used for ablation, the fs laser shows many unique characteristics including negligible cracks, minimal heat-affected-zones, low recast, and high precision. The merits of this advanced manufacturing technique provide the unique opportunity to fabricate novel microsensors with enriched functionality, enhanced intelligence, and unprecedented performance.

The laser employed in this research was a Ti:Sapphire fs laser system manufactured by Coherent Inc. The performance specifications for the laser are summarized in Table 3.1. The full ultrafast laser system consists of a diode-pumped solid state laser with high power CW output at 532 nm (Verdi V18, Coherent Inc.), a Ti:Sapphire mode-locked laser (Mira 900, Coherent Inc.) and a Ti: Sapphire regenerative amplifier laser (RegA 9000, Coherent Inc.). The schematic of our home-integrated fs laser micromachining system with direct writing capability is shown in Fig. 3.1. The central wavelength, pulse width, and repetition rate of the fs laser set at 800 nm, 200 fs, and 250 kHz, respectively. The maximum output power of the fs laser is 1 W, so the single pulse energy is around 4 μJ [87].

Table 3.1. Femtosecond laser system specifications

SPECIFICATIONS*		
Model No.	Mira 900 (Oscillator)	RegA 9000(Amplifier)
Pump Power	8 W	10 W
Pulse Duration	200 fs	200 fs

Pulse Energy	2 μJ	2 μJ
Wavelength Range	700-980 nm	400-1000 nm
Average Power	1 W	500 mW
Repetition rate	76 MHz	10 kHz to 300 kHz
Beam Diameter	0.8 ± 0.1	3 mm
Beam Divergence	1.7 ± 0.2 mrad	3 mrad

*Provided by the manufacturer

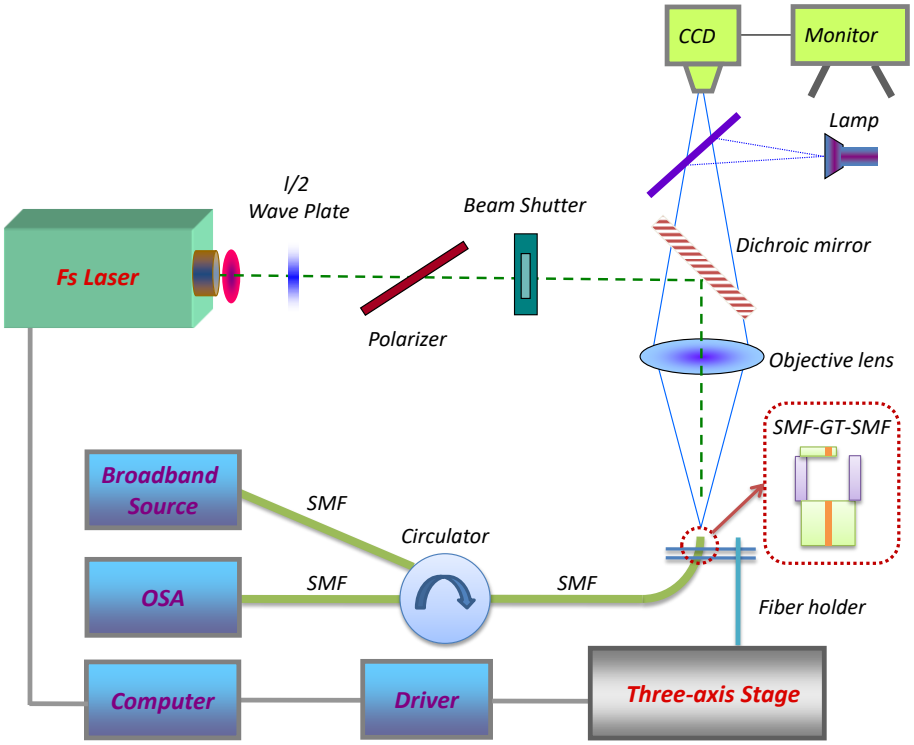

Fig. 3.1. Schematic of the fs laser micromachining system.

For the beam delivery optics, a half waveplate in combination with a Glan-Thompson Calcite polarizer is used to precisely control the actual power used for fabrication, while an optional variable neutral density (ND) filter is used to tune the laser power more precisely. The laser exposure is switched on or off by an external mechanical

shutter (SH05, Thorlabs) or electrically gating the internal clock via laser controller. In general case, the laser beam is passed through a commercial microscope objective to create a tightly focused spot. The actual laser energy used for processing SMF-GT-SMF structure is approximately 0.4 μJ per pulse.

3.1.3 Micro-cantilever fabrication

During fs laser micromachining, the prepared SMF-GT-SMF structure was vertically mounted on a fiber holder shown in Fig. 3.2. Then, the whole parts were mounted on a high-precision computer-controlled three-axial translation stage (Newport, Inc.) with a resolution of 0.1 μm. The fs laser beam was focused onto the endface of the SMF-GT-SMF structure through an objective lens (Zeiss EC Epiplan, 20X) with a numerical aperture (NA) of 0.4 shown as Fig. 3.3. The spot size of the focused beam was about 1 μm. An in-situ monitoring system was used to monitor the performance of the device during the micromachining process. The monitoring system consists of an erbium-doped fiber amplified (EDFA) spontaneous emission broadband light source (1520–1620 nm), a fiber circulator, and an optical spectrum analyzer (OSA, AQ6319), as shown in Fig. 3.4.

The diaphragm thinning process was performed layer-by-layer with a step size of 2 μm. The fabrication was completed when the preset depth scan was reached. Then, the 3D customized image scanning was also performed layer-by-layer with a step size of 0.5 μm. The shape and depth of the fabricating structure could be varied flexibly. The ablation process was stopped after the desired thickness of the diaphragm structure was achieved.

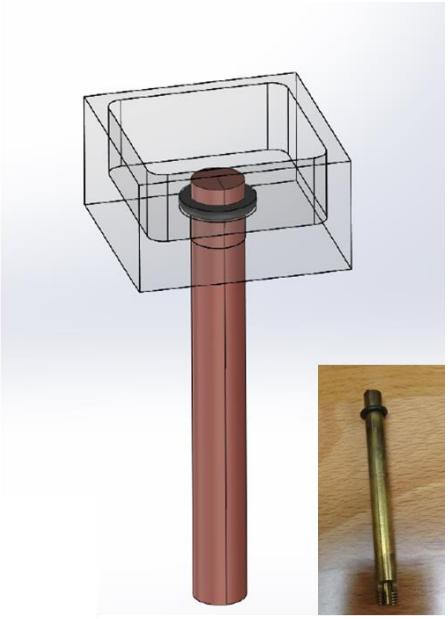

Fig. 3.2. The holder used in an fs laser micro-machining system.

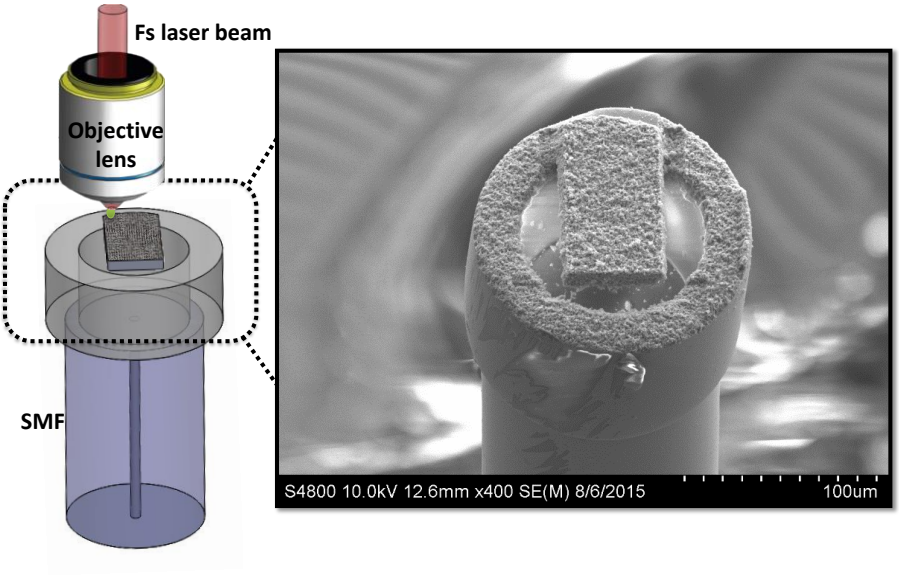

Fig. 3.3. Schematic diagram of the fs laser micro-machined micro-cantilever and SEM image of the top-viewed micro-cantilever.

It should be noted that the FP cavity can also be formed by fs laser ablation or the drilling process followed by fusion splicing to another piece of SMF and the

thinning/roughening process of the diaphragm structure, as shown in Ref [30]. Such a structure had a uniform diameter in the cross section along the fiber axis, but the cavity length might be limited by the Gaussian shape of the laser beam.

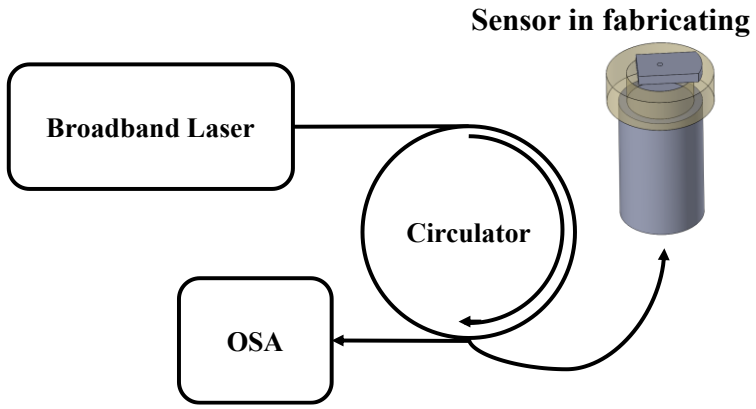

Fig. 3.4. The schematic of monitoring system.

In addition, the micro-cantilever beam was ablated based on the diaphragm structure using the fs laser ablation process. The shape of the micro-cantilever beam can be well controlled by moving the high-precision three-axial translation stage. The ablating process was not stopped until the desire shape of the micro-cantilever beam was formed. After the cantilever beam fabrication, the interference signal was not as good as we expected due to the debris of the fiber generated during the fabrication process. To obtain a high-quality interference signal, the structure was then subjected to slight cleaning with ethanol flow. Fig. 3.5(b) shows the interference spectrums improved after cleaning.

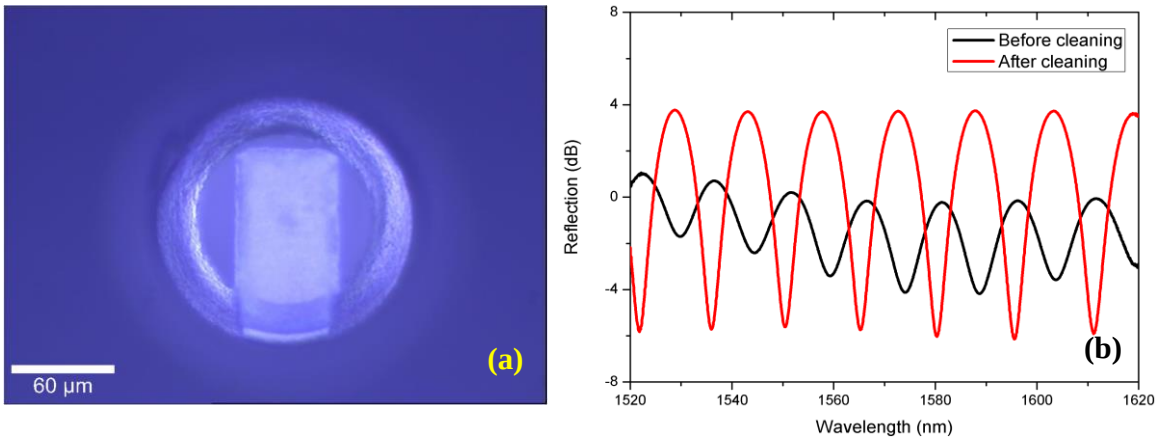

Fig. 3.5. (a) A rectangular cantilever beam fabricated by fs laser micromachining system. (b) The reflection spectra before and after cleaning.

3.2 Acoustic sensor test in air [85]

The micro-cantilever beam was ablated based on the diaphragm structure (as shown in Ref [30]) using the fs laser ablation process. Fig. 3.6 shows the side-view of microscopy image of the micro-cantilever based optical fiber sensor, and the top-view of microscopy image of the rectangular shaped cantilever with the thickness of ~5 μm is shown in the inset of Fig. 3.6. The interference spectra (before and after cleaning) are shown in Fig. 3.5(b). The reflection spectrum of the fabricated structure after cleaning shows a clean interference pattern with a large fringe visibility of about 10 dB, which is adequate for most sensing applications. We did not see any wavelength shift when external pressure was applied to the sensor head, which indicated that the Q-point drift issue could be ignored. The acoustic wave interrogation system is shown in Fig. 3.7. The interrogation unit includes the following components: a tunable laser (HP8164A, Agilent, Inc.) as the light source, an erbium-doped fiber amplifier (EDFA, INO, Inc.) to amplify the optical signal, a

photodetector to convert the optical signal to the electrical signal, and an oscilloscope (DPO7254,Tektronix) to analyze the signal. The light from the tunable laser was coupled into the sensor through a circulator. The reflected signal from the sensor head was collected by using the same circulator, transferred by using a photodetector, and analyzed by using the oscilloscope. The input acoustic signal was excited by a speaker combined with a function generator. The sensor was measured in the frequency range of 100 Hz – 4 kHz by using the sinusoidal signal. After getting the interference spectrum, the operating point was chosen at 1538.52 nm, as shown in Fig. 3.8. Based on the free spectrum range of the interferogram, the cavity length of the sensor is estimated to be 65.9 μm. The sensor frequency response curve in the frequency range of 100 Hz – 3.2 kHz is plotted in Fig. 3.9. The resonance frequency of the sensor is in the MHz range, and so, the 100 Hz – 3.2 kHz frequency range is approximately in the linear response region of the sensor in theory. Because the acoustic source cannot guarantee to provide constant intensity at different frequencies and there is no reference microphone available, the frequency response cannot be normalized as shown in Fig. 3.9. However, it demonstrates that the sensor responses well to acoustic signals in the low frequency range. Representative result at 1 kHz is shown in Fig. 3.10. The results demonstrate the high response in the low frequency range of the sensor.

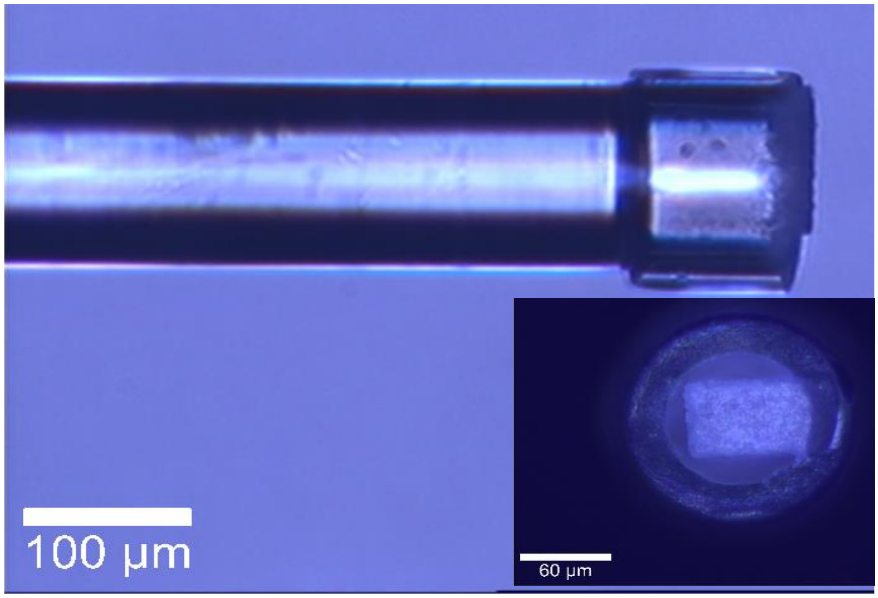

Fig. 3.6. Side-view of the microscopy image of the micro-cantilever based FP acoustic sensor (inset: top-view of the rectangular shaped micro-cantilever beam).

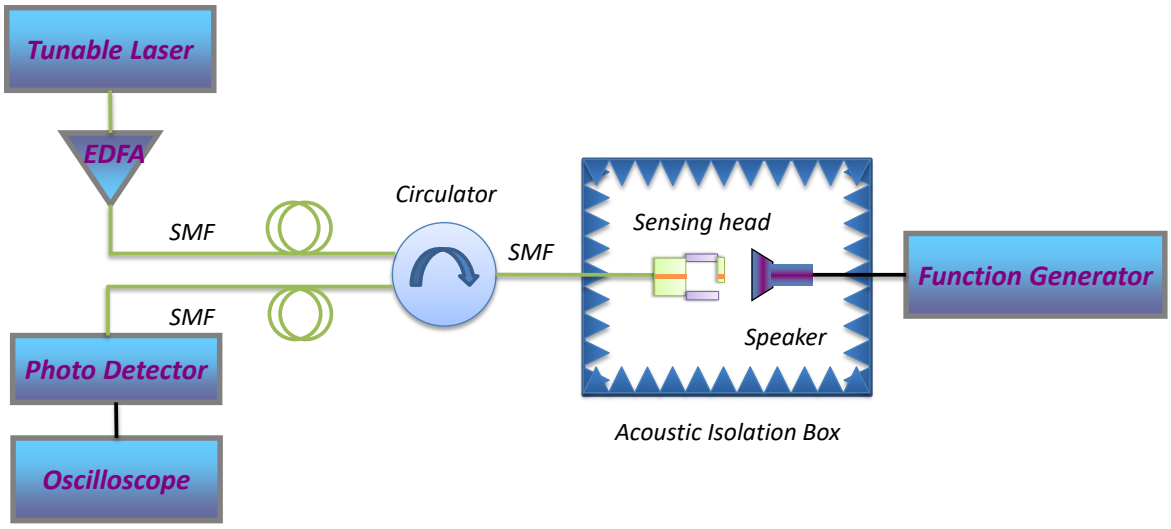

Fig. 3.7. Experimental setup of the interrogation system.

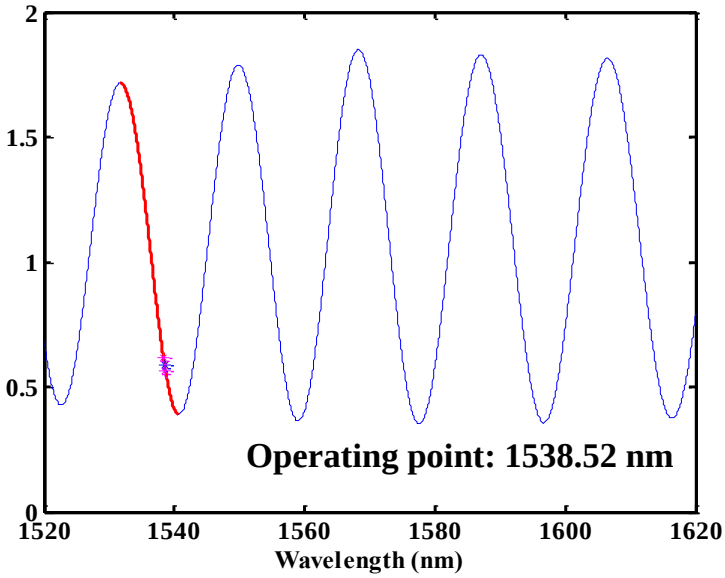

Fig. 3.8. The interference spectrum of the sensor in air, operating point is chose at 1538.52 nm.

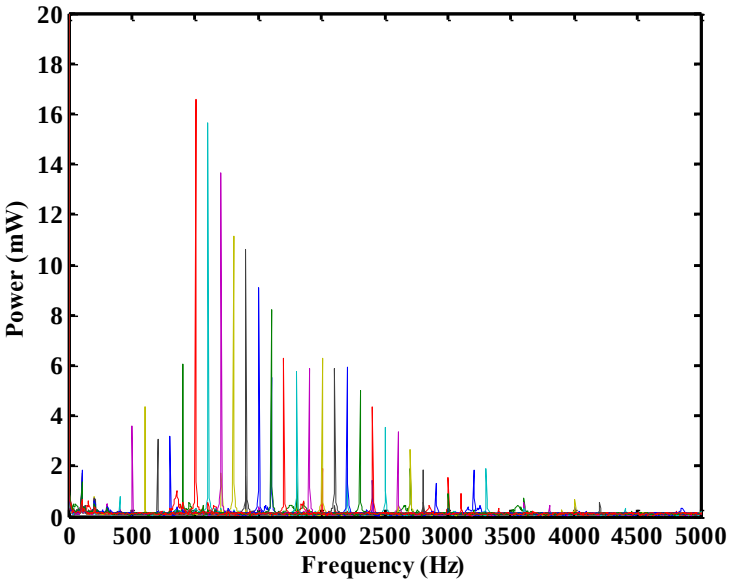

Fig. 3.9. Frequency response spectrum of the acoustic sensor.

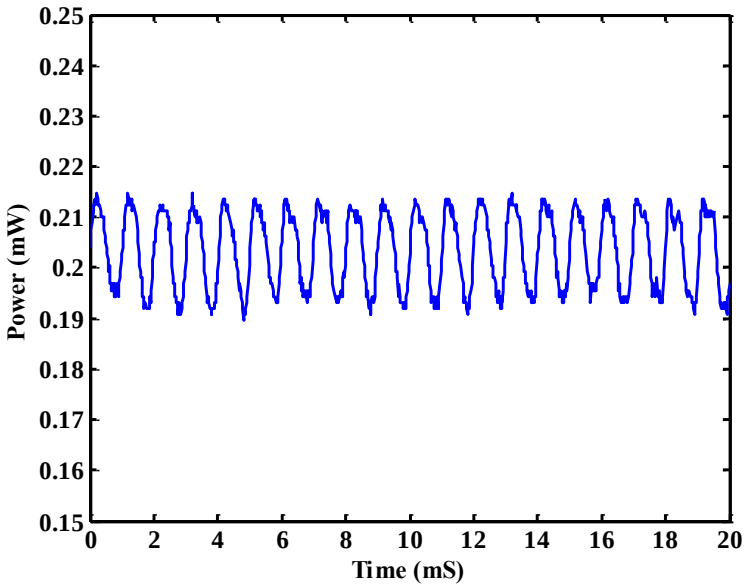

Fig. 3.10. The time domain signal of the sensor was applied 1 kHz acoustic wave.

In summary, the fs laser fabricated pure silica micro-cantilever based optical fiber acoustic sensor was investigated for the acoustic wave measurement. The sensor has been tested in low frequency acoustic signals in air. Based on the micromachining capability of the fs laser, different structures of the optical fiber sensors would be further explored. In addition, the sensing performance of this proposed sensor operating in water were also investigated.

3.3 Hydrophone test in water [81]

Figure 3.11 shows the calculated deflection of the micro-cantilever beam as a function of the excitation frequency. The deflection is normalized by setting the amplitude of the driving force A equal to 1. The length L, width b and thickness h of the micro-cantilever beam are set at 75 μm, 50 μm and 8 μm in the calculations, respectively. Other

parameters used in the simulation include the Young's modulus of 73 GPa, the Poisson's ratio of silica of 0.17, and the viscosity coefficient of water of 2.5e-3 Pa·s. As shown in Fig. 3.11, the fundamental frequency of vibration of the micro-cantilever beam in water is 0.72 MHz and the second mode frequency is 4.5 MHz.

A micro-cantilever based FOH is fabricated according to the dimensions used in numerical simulation shown in Fig. 3.11.

Figure 3.12 shows the test setup. The light from the tunable laser (HP8164A, Agilent Inc.) was coupled into the sensor through a circulator. The reflected signal from the sensor head was collected by the same circulator and detected by a photodetector (P6703B, Tektronix), and analyzed by the oscilloscope (DPO7254, Tektronix). The input acoustic signal was excited by an ultrasonic immersion transducer (OLYMPUS) driven by the function generator (Agilent, 33120A) and the RF amplifier (Amplifier Research, 75A250A). The ultrasonic signal strength was calibrated using another immersion transducer from OLYMPUS at the location where the fiber sensor was to be tested. A three-dimensional stage was used to hold the transducer and adjusted the position between the transducer and the FOH. Both the transducer and the sensor were immersed into the deionized water.

We first used the optical spectrum analyzer (OSA) to record the sensor spectra as shown in Fig. 3.13 and set the tunable laser wavelength to be at 1543.3 nm. This wavelength was chosen to allow the sensor operating at the quadrature point for maximum sensitivity. No obvious operating point drift was found when varying the immersion depth of the sensor under the water.

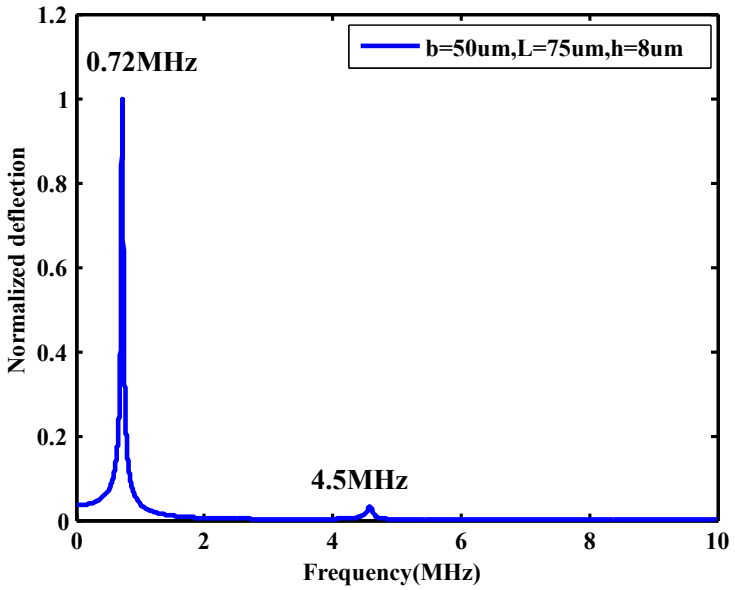

Fig. 3.11. Calculated deflection of the micro-cantilever beam immersed in water as a function of the acoustic wave frequency.

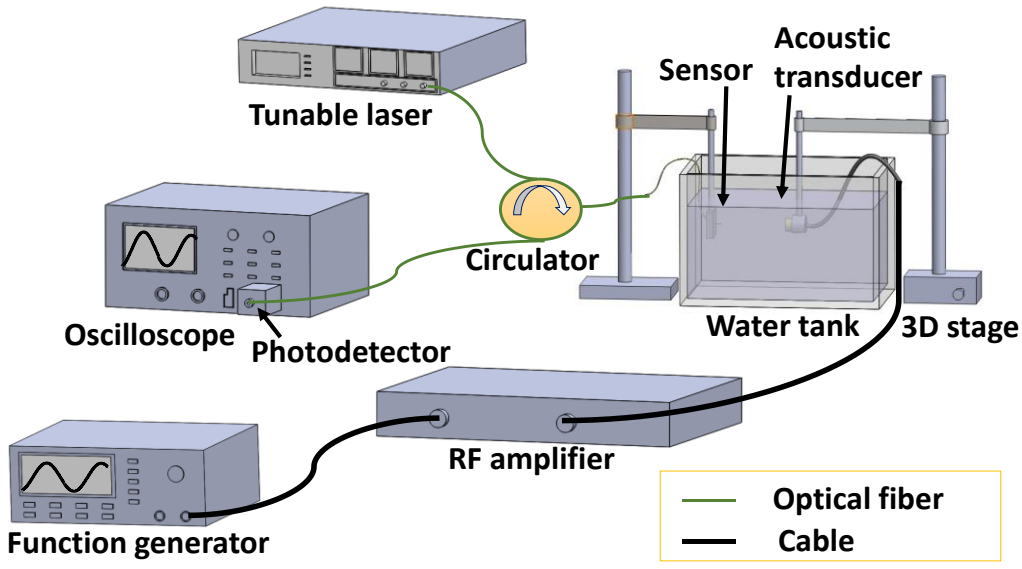

Fig. 3.12. Experimental setup to test the sensor response to underwater acoustic waves.

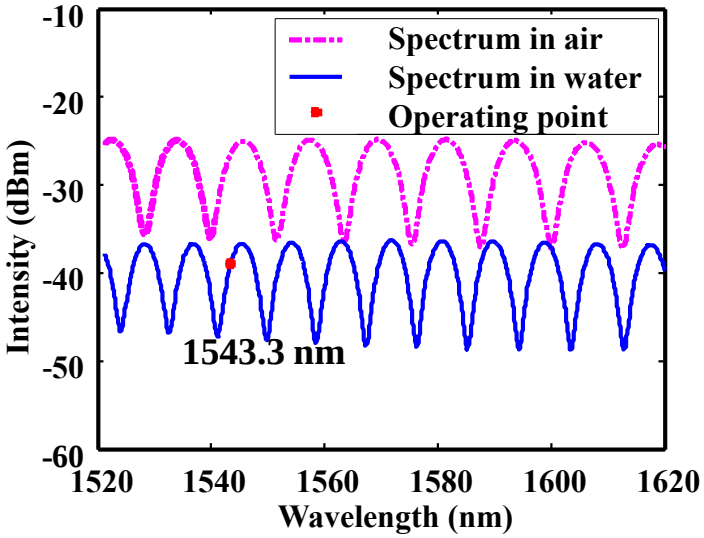

Fig. 3.13. Interference spectra in air (dashed line) and water (solid line).

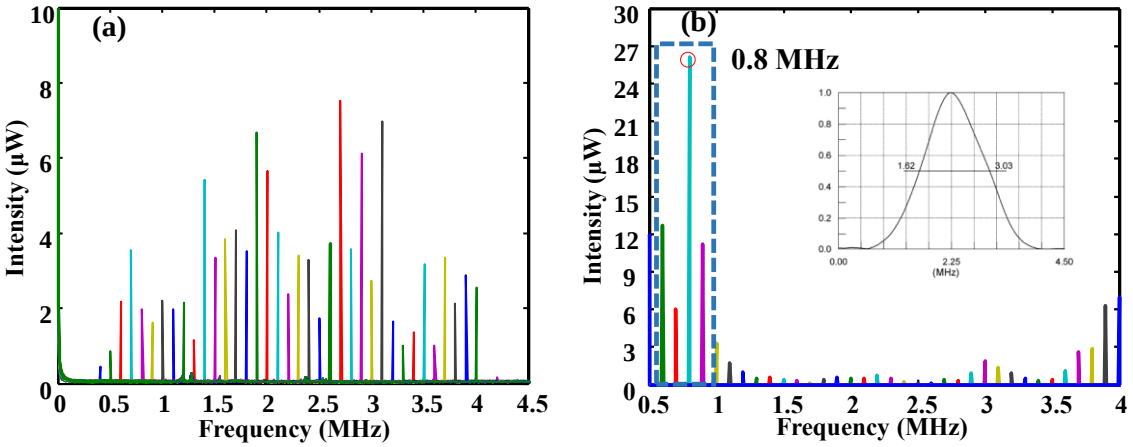

Fig. 3.14. (a) Original frequency response of the sensor in the range of 0.5 – 4 MHz. (b) Normalized frequency response of the sensor. Inset: frequency response of the OLYMPUS transducer used in the experiment.

Based on the calculation result shown in Fig. 3.11, an ultrasonic transducer with the center frequency of 2.25 MHz was chose to test the frequency response of the sensor. The swept frequencies went through the entire available range of 0.5 - 4 MHz with the step

of 0.1 MHz. Each measurement was repeated 5 times and the average value was taken as the result. The original frequency spectrum were normalized by the transducer frequency spectrum shown in the inset of Fig. 3.14(b).

Figure 3.14(a) shows the original frequency response, Fig. 3.14(b) shows the normalized frequency response of the micro-cantilever based FOH in range of 0.5 - 4 MHz. The highest response occurred at 0.8 MHz. We then used a finer step of 0.01 MHz to scan through the range of 0.5 - 0.9 MHz using another transducer with the center frequency of 0.5 MHz and the normalized frequency response of the fiber optic sensor is shown in Fig. 3.15. The resonant frequency of the proposed sensor is around 0.74 MHz, which is in a good agreement with the simulated of 0.72 MHz. The small difference between the measured and calculated resonant frequencies might be caused by the slight differences in dimensions of the fabricated and modeled cantilevers. The full width at half maximum (FWHM) of the sensor was estimated to be 0.021 MHz. The representative time domain signal received by the hydrophone at 0.74 MHz is shown in Fig. 3.16(b). The frequency spectrum of the sensor is shown in Fig. 3.16(a) where the signal noise ratio (SNR) is estimated to be about 23 dB based on the peak intensity (-28 dBm) and noise level (-51 dBm). Additionally, Fig. 3.16(a) also indicates that the hydrophone is operating at the highest input power.

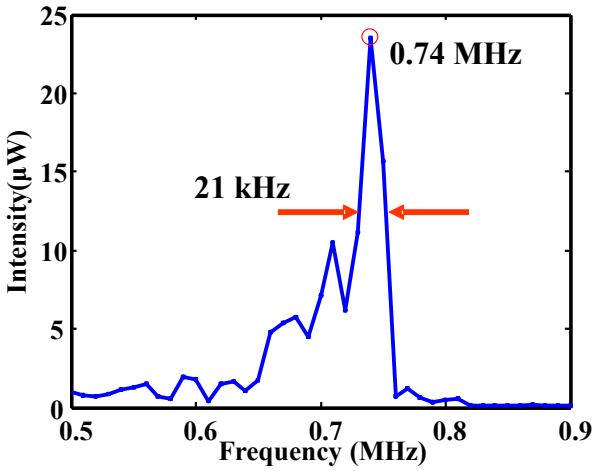

Fig. 3.15. Zoomed-in response spectrum of 3.14(b) in the range of 0.5-0.9 MHz.

The hydrophone was then measured over a range of acoustic pressures by varying the input power to the immersion transducer that was used to generate the acoustic waves. The acoustic pressure was calculated based on the input power of the immersion transducer [88]. The amount of deflection of the cantilever beam was calculated based on the intensity variation of the hydrophone. According to interference spectrum shown in Fig. 3.13, the intensity variation can be further used to calculate the corresponding cavity length change of the FPI. The amount of beam deflections are plotted as a function of the applied acoustic pressure as shown in Fig. 3.17, where the sensitivity is estimated, based on the slope of the linear-fit of the calculated data, to be about 9.75 μm/MPa at the resonant frequency of 0.74 MHz. If we assume that the sensor can resolve a signal that is equal to the noise, the detection limit (SNR=1) of the sensor operating at the highest input power is estimated to be about 491.2 Pa at the resonant frequency of 0.74 MHz.

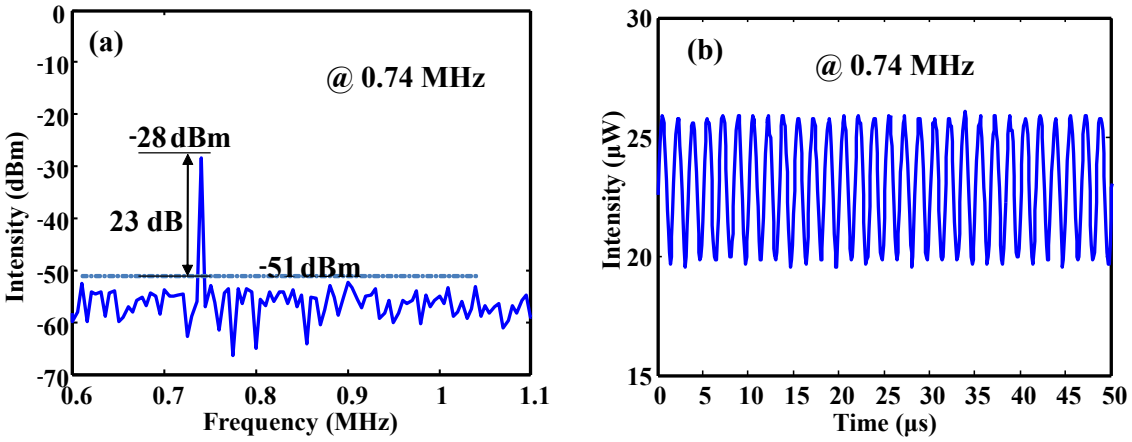

Fig. 3.16. (a) Frequency and (b) time responses of the sensor at the resonant frequency 0.74 MHz.

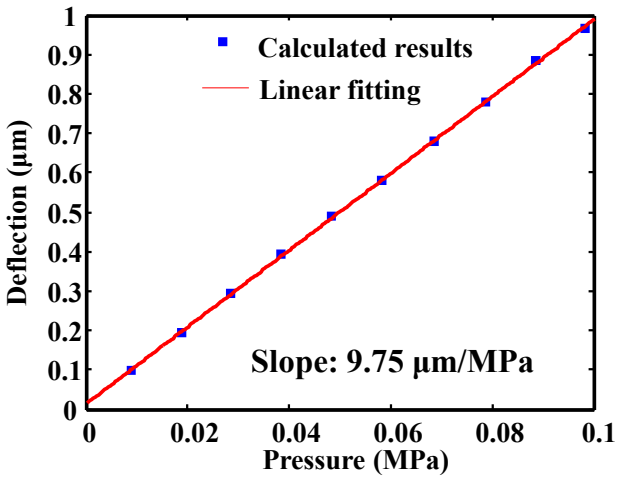

Fig. 3.17. Deflection of the micro-cantilever as a function of the applied acoustic pressure.

3.4 Conclusion

In summary, an open cavity, micro-cantilever based fiber optic FPI hydrophone was fabricated by high precision fs laser micromachining. The sensor was theoretical

analyzed and experimentally tested to investigate its frequency response when immersed in fluid. The device has a miniaturization level, large response near the resonant frequency and no operating point drift when the immersion depth varies. The resonant frequency of the proposed device can be predicted and fine-tuned by changing the dimension of the micro-cantilever. The simulated dynamic responses of the sensor agree well with the experimental results. It is believed that cantilever-based FOH may find potentially useful for endoscopic photoacoustic imaging.

CHAPTER FOUR

V-SHAPED AND TRIANGULAR CANTILEVER BASED FOHs

4.1 Introduction

Fs laser micromachining system provide a great opportunity to precisely realize various shapes and dimensions of micro-cantilever fabrication. For the sake of effective fabrication, the resonant frequencies and dimensions of the micro cantilever need to be predesigned and pre-calculated.

Figure 4.1 shows structures of three different shapes of cantilevers with same length L and same thickness h. The width of rectangular cantilever are two times of one arm of V-shaped cantilever. The resonant behavior of a cantilever with an arbitrary shape can be obtained based on Rayleigh-Ritz method [77]. For immersion application, the finite element analysis with COMSOL was done to predict the resonant response of the structure.

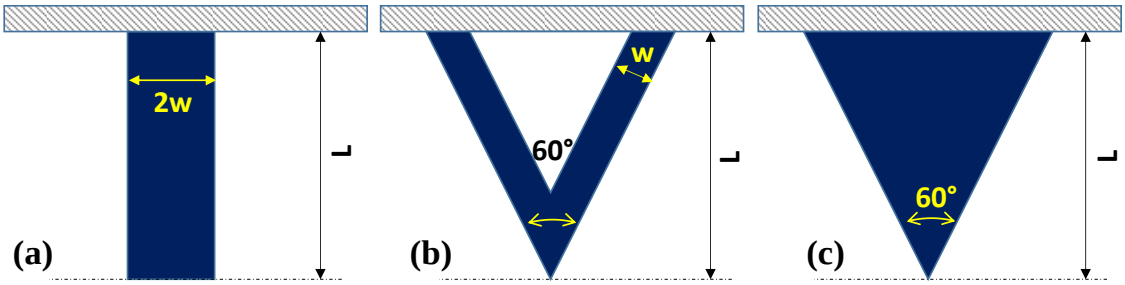

Fig. 4.1. Shape and dimensions of (a) rectangular cantilever (b) V-shaped cantilever and (c) triangular cantilever.

The parameters required in the simulation include Young's modulus E = 73 GPa, Poison's ratio ν = 0.17 and density ρ = 2300 kg/m^3 of fused silica. The dimensions of the structures include length L = 70 μm, thickness h = 10 μm. The width of one arm of the V-

shaped cantilever w = 25 μm. The resonant frequencies in vacuum were calculated from equations. For immersion case, the fluid affects the mode shapes and the resonant behavior of the cantilever structures. COMSOL can help us in modelling and to find out the resonant frequencies of the immersed cantilever beams under viscous effects. Numerical simulated and finite element simulated with COMSOL results are all shown in table 4.1, which indicate the frequency increased after changing the shape from rectangular cantilever to V-shaped or triangular cantilevers. Triangular cantilever has the biggest resonant frequency compared the other two shapes of cantilevers. Immersing in water would reduce the resonant frequencies. The first mode shapes of immersed V-shaped and triangular cantilever beams are shown in Fig 4.2 and 4.3 respectively.

Table 4.1 Comparison of resonant frequencies of different cantilevers in fluid got from different methods

Shape of cantilever	Resonant frequency in vacuum calculated (MHz)	Resonant frequency in water (COMSOL) (MHz)
Rectangular	1.32	0.84
V-shaped	2.45	1.50
Triangle	2.7	1.75

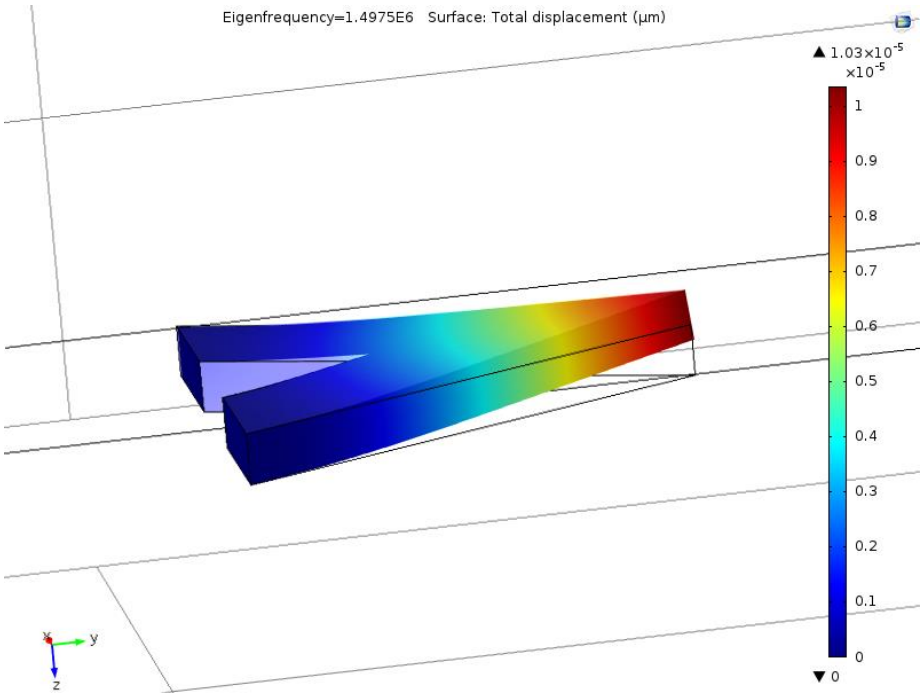

Fig. 4.2. The first mode shape of immersed V-shaped micro-cantilever.

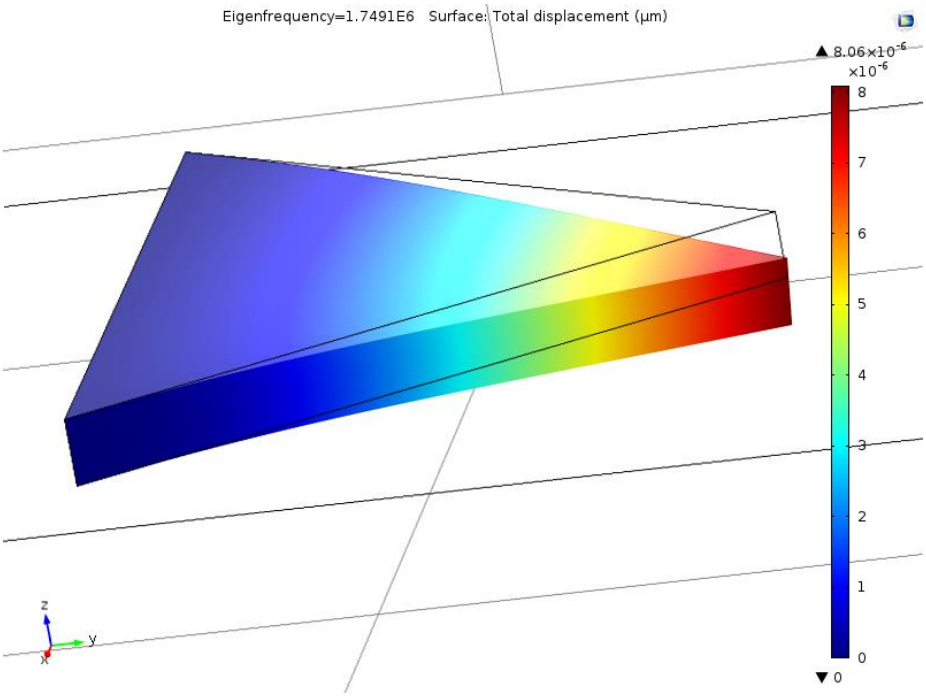

Fig. 4.3. The first mode shape of immersed triangular micro-cantilever.

4.2 Fabrication of the V-shaped and triangular cantilever based FOH

An EFPI was first fabricated at the tip of a SMF following the procedure outlined by Ref. [81]. In Chapter three, the fabrication of the rectangular cantilever based FOH has been described clearly. With the help of fs laser, V-shaped and triangular cantilever hydrophones were finished and shown in Fig. 4.4(a) and (b), dimensions and shapes of two different cantilevers were precisely controlled. The effective length of those two structure was about 70 μm. Each arm of the V-shaped cantilever was 25 μm width, and it had a 60° angled tip, so as the triangular cantilever. The thickness of these two micro-cantilever was about 10 μm.

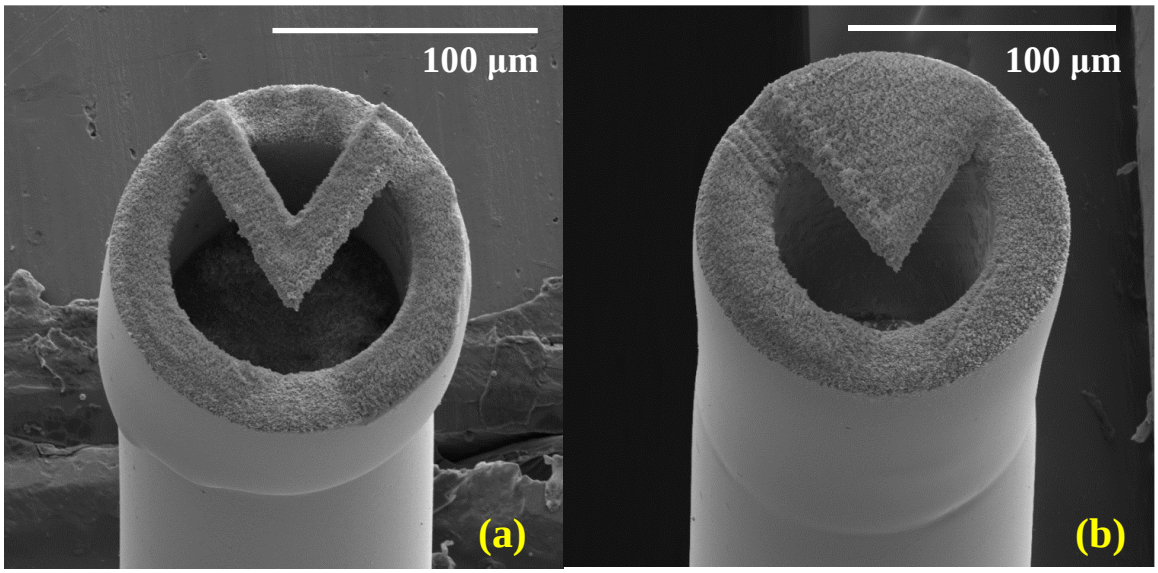

Fig 4.4. SEM images of (a) V-shaped cantilever and (b) triangular cantilever.

4.3 Hydrophones test in water

In order to experimental investigate the properties of optic fiber hydrophones, frequency response testing was conducted using the setup system as shown in Fig. 3.12.

4.3.1 V-shaped cantilever based FOH test in water

The reflection spectrum of the V-shaped cantilever based FOH was recorded by the OSA and is shown in Fig. 4.5. The operating point was chose at 1537.7 nm for maximum sensitivity. The cavity length calculated from the interference spectrum was about 46 μm.

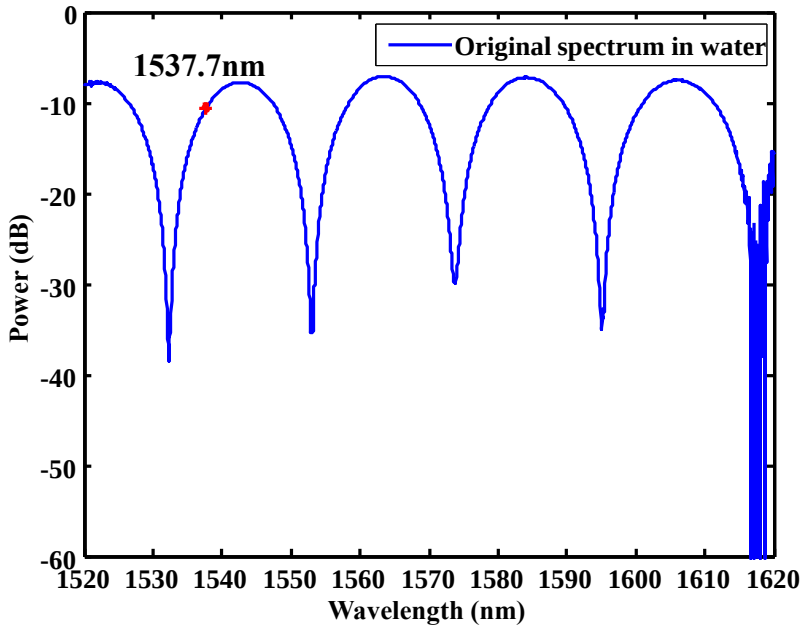

Fig. 4.5. Reflection spectrum of V-shaped cantilever based FOH in water.

From the finite element analysis result shown in table 4.1, the resonant frequency of the hydrophone is near to 1.5 MHz, so the center frequency of 2.25 MHz immersion transducer was chose to test the hydrophone. The frequency response evaluated was from 0.5 MHz to 4 MHz with step of 0.1MHz. Due to the performance of the immersion transducer is not consistent under all the frequency range, the frequency responses of the sensors gained in experiments need to be normalized by the frequency spectrum of the immersion transducer used as acoustic signal source, which are shown in the inset of the Fig. 3.14(b). The original frequency response and normalized spectrum are shown in Fig.

4.6. It is obviously that the resonant frequency of the hydrophone is around 1.3 MHz. In order to find out much more accurate value of the highest response of the hydrophone, dynamic response of the hydrophone was subtly tested with step of 0.01 MHz in range of 1-2 MHz. Figure 4.7(a) shows zoomed in response spectrum of Fig. 4.6(a) in range of 1-2 MHz, the normalized spectrum is shown in Fig. 4.7(b). The resonant frequency is around 1.36 MHz, which is in agreement with the simulated result of 1.5 MHz shown in table 4.1. The full width at half maximum of the hydrophone is about 0.29 MHz shown in Fig. 4.8. The representative time domain signal and frequency domain signal at resonant frequency of 1.36 MHz are shown in Fig 4.9(a) and (b). The SNR approaches 27 dB based on the peak intensity of -28 dBm and noise level of -55 dBm.

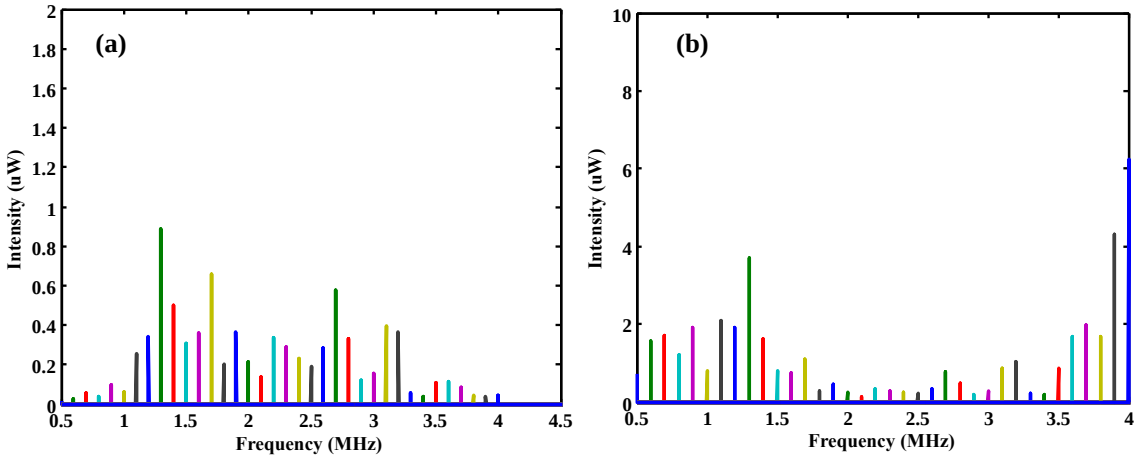

Fig. 4.6. (a) Original frequency response of the hydrophone in the range of 0.5-4 MHz. (b) Normalized frequency response of the sensor.

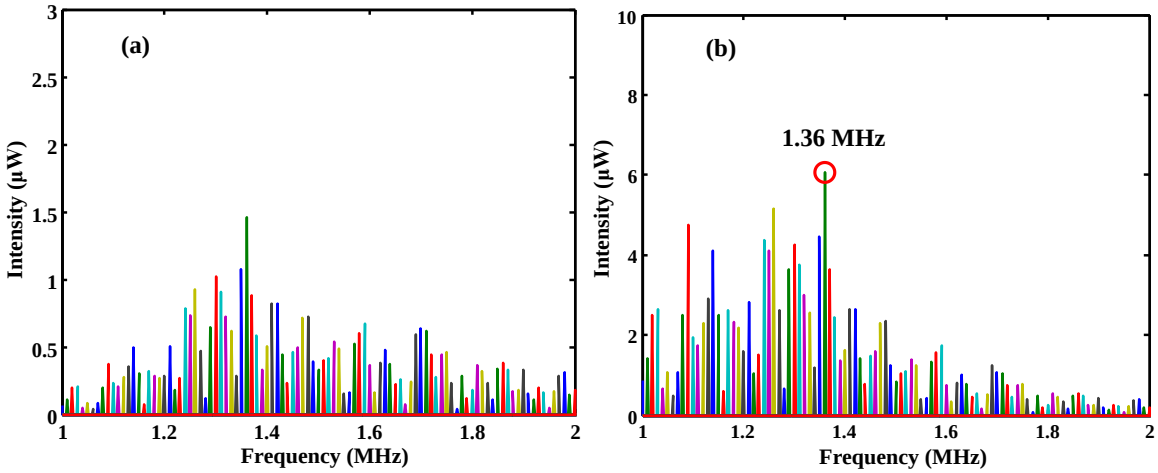

Fig. 4.7. (a) Original frequency response of the hydrophone in the range of 1-2 MHz. (b) Normalized frequency response of the sensor.

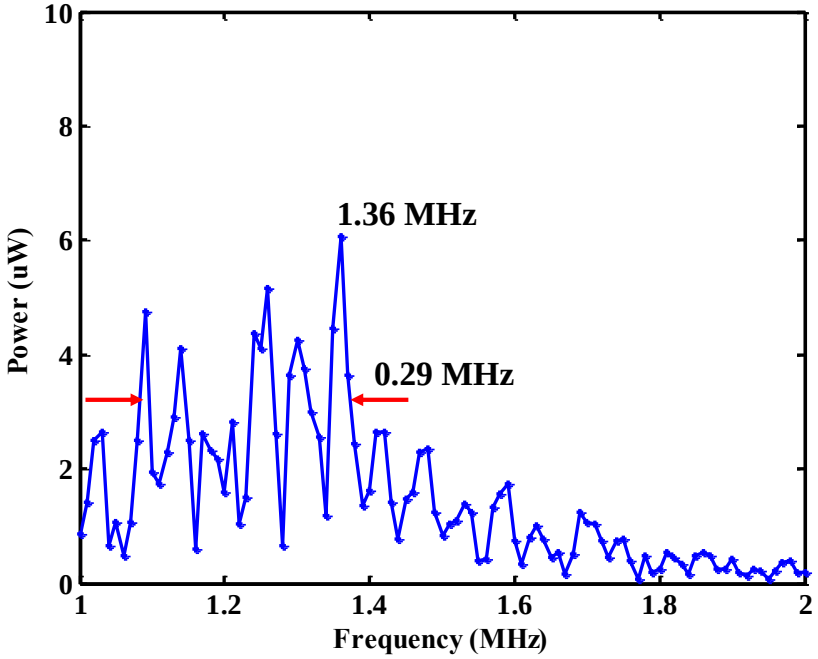

Fig. 4.8. Zoomed-in response spectrum of 4.6(b) in the range of 1-2 MHz.

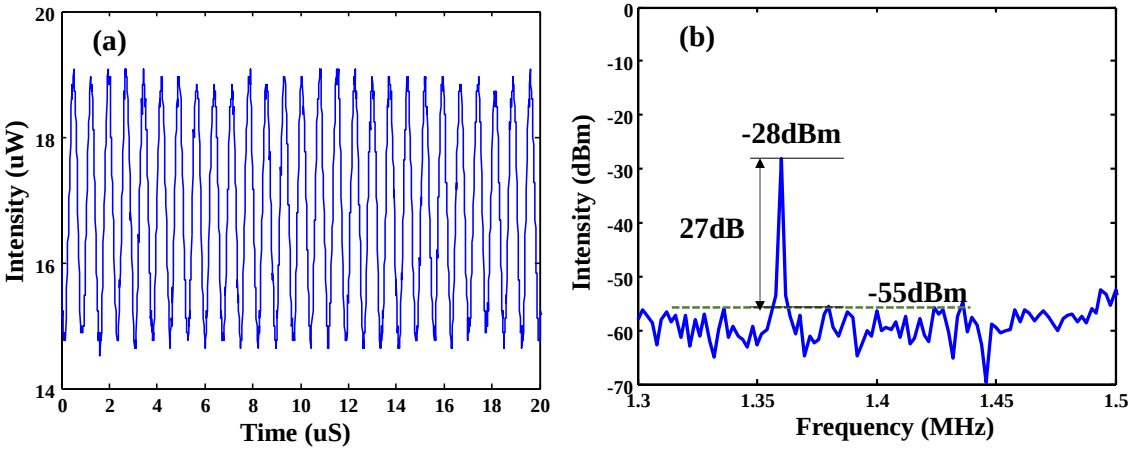

Fig. 4.9. (a) Time domain signal and (b) frequency spectrum of the hydrophone at the resonant frequency of 1.36 MHz.

The sensitivity of the hydrophone was measured by changing input power of the immersed acoustic transducer used as acoustic source. Applied acoustic pressures are calculated from input power of the acoustic source. The output signals of the hydrophone could be used to work out maximum deflections of the sensing part under different acoustic pressures according to the slop of 4.12e-6 μW/nm around the operating point shown in Fig 4.10(a). The amount of beam deflections are plotted as a function of the applied acoustic pressure as shown in Fig. 4.10(b), where the sensitivity is estimated to be about 105 nm/MPa according to the slope of the linear fitting of the calculated results. The detection limit of the hydrophone is about 410 Pa at the resonant frequency of 1.36 MHz.

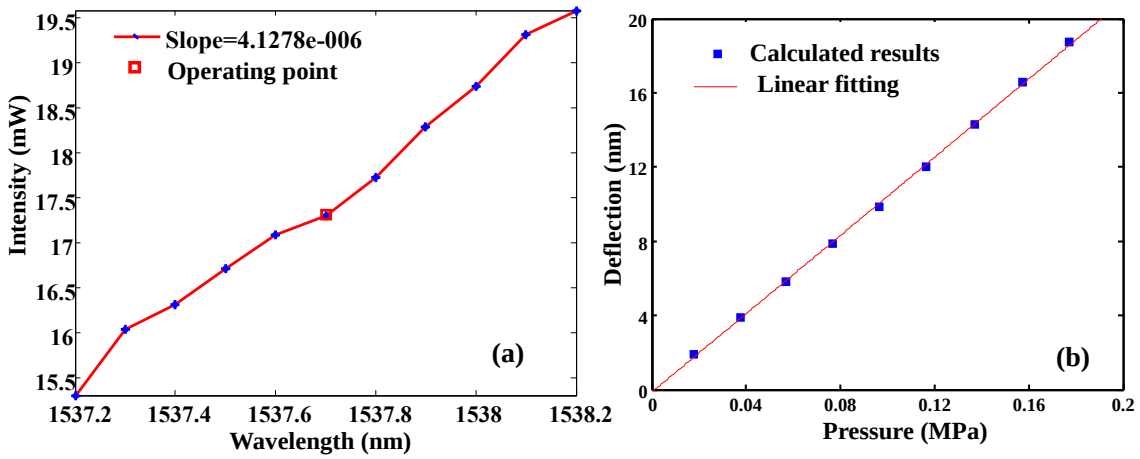

Fig. 4.10. (a) Interference spectrum of the hydrophone around the operating point, (b) Deflection of the V-shaped micro-cantilever as a function of the applied acoustic pressure.

4.3.2 Triangular cantilever based FOH test in water

The interference spectrum of the triangular cantilever based FOH is shown in Fig. 4.11, the operating point is chose in the largest slope section of spectrum as 1530.6 nm.

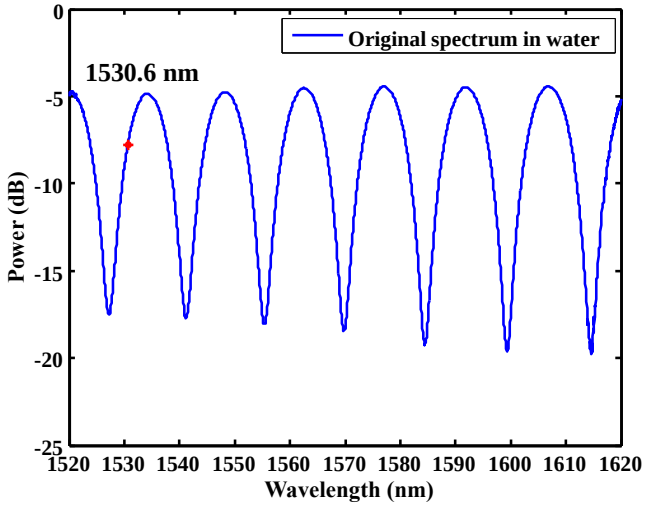

Fig. 4.11. Interference spectrum of triangular cantilever based FOH in water.

The EFPI cavity length of the hydrophone is estimated from the interference spectrum to be 65 μm. The resonant frequency of the triangular cantilever is bigger than it of the V-shaped cantilever based on finite element analysis results with COMOSL shown in table 4.1. The triangular cantilever would be much easier in fabrication and has much better reflection compared with V-shaped cantilever beam, because the triangular shape has larger reflection area.

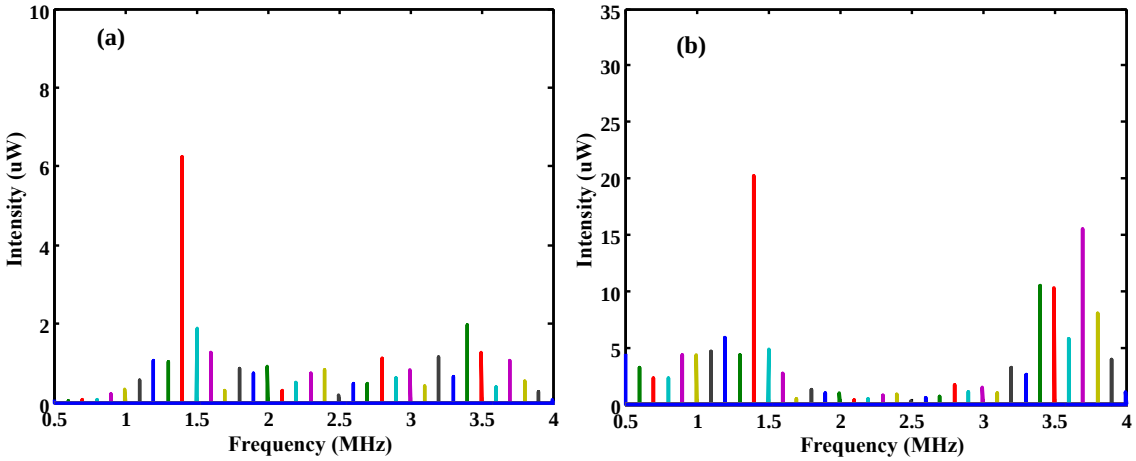

Fig. 4.12. (a) Original frequency response of the hydrophone in the range of 0.5-4 MHz. (b) Normalized frequency response of the sensor.

The frequency response of the hydrophone was tested in range of 0.5-4 MHz with step of 0.1 MHz. The original frequency response is shown in Fig 4.12(a), and the normalized spectrum is shown in Fig. 4.12(b). The resonant frequency of the hydrophone should be around 1.4 MHz from Fig. 4.12(b). Zoomed-in spectrum of 4.12(b) is shown in Fig. 4.13(b), the original spectrum is shown in Fig. 4.13(a), which is obtained by sweeping in range of 1.1-1.8 MHz with step of 0.01 MHz. Obviously, the resonant frequency of the

triangular cantilever based FOH is 1.39 MHz, which is near to the simulated result of 1.75 MHz shown in table 4.1.

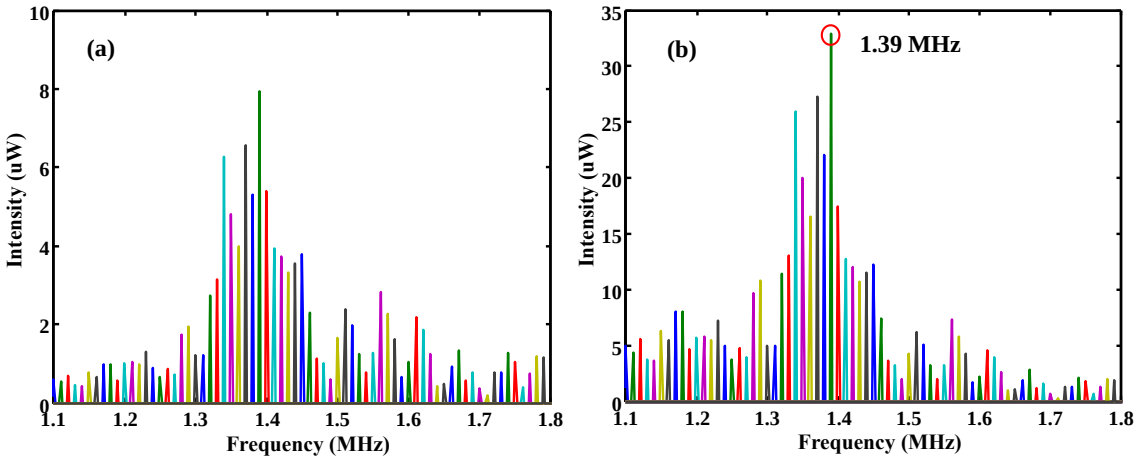

Fig. 4.13. (a) Original frequency response of the hydrophone in the range of 1.1-1.8 MHz. (b) Normalized frequency response of the hydrophone.

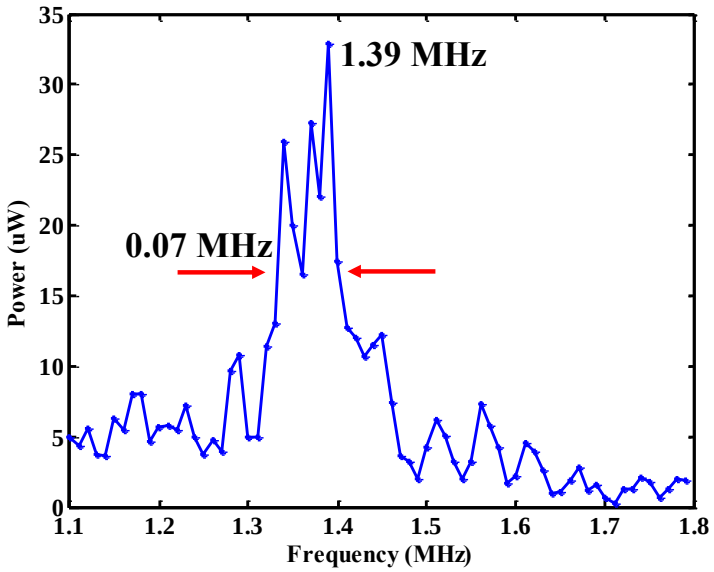

Fig. 4.14. Zoomed-in response spectrum of 4.12(b) in range of 1.1-1.8 MHz.

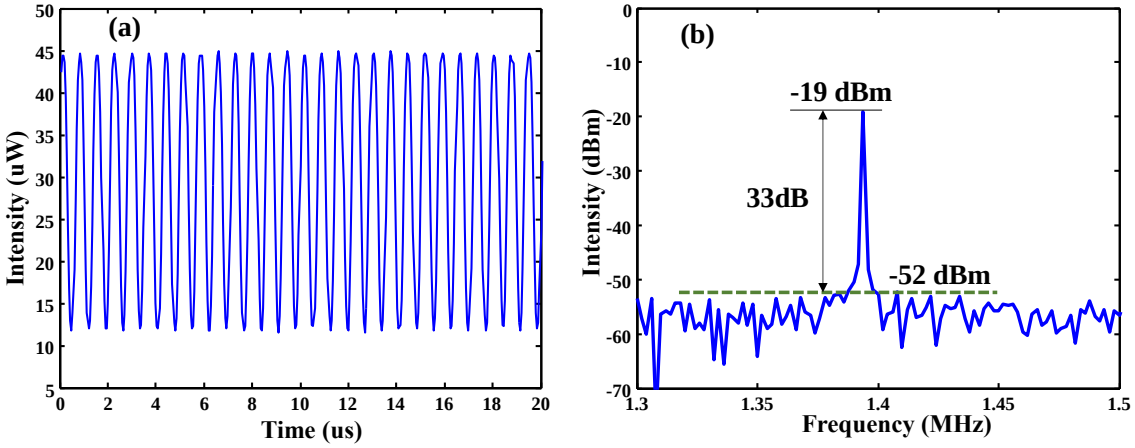

Fig. 4.15. (a) Time domain signal and (b) frequency spectrum of the hydrophone at the resonant frequency of 1.39 MHz.

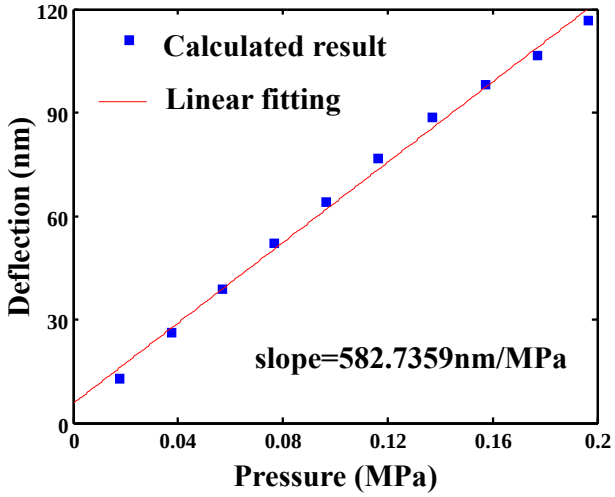

Fig. 4.16. Deflection of the triangular cantilever as a function of the applied acoustic pressure.

Figure 4.14 shows the FWHM of the hydrophone is about 0.07 MHz. At resonant frequency of hydrophone, the representative time domain and frequency domain signals are shown in Fig. 4.15(a) and (b). The SNR is 37 dB based on peak intensity of -19 dBm and noise level of -52 dBm. The sensitivity of the hydrophone is calculated and presented

in Fig. 4.16 as 582.7 nm/MPa based on linear fitting. The detection limit of the hydrophone is calculated to be 102 Pa at the resonant frequency of 1.39 MHz.

4.4 Conclusion

V-shaped and triangular cantilever based FOHs with the almost same length and same thickness would have 1.3 MHz and 1.4 MHz resonant responses respectively. Changing shapes of cantilever would be much more effective method to improve the frequency response of the cantilever based FOH.

Cantilever based FOH is a high-Q sensor, which means it has a narrow bandwidth. Sensitivities of the hydrophones are shown as Fig. 3.17, Fig. 4.10(b) and Fig. 4.16, which are almost in the same level. Sensitivity of the sensor mainly depends on the dimensions and material of the sensing element, the three different cantilever based FOHs have same material and same scale sensing micro cantilever structure, which make the sensitivity wouldn’t change a lot.

Micro-cantilever structure are optimized from rectangular to V-shaped and triangular cantilevers for increasing resonant frequency, which should be an effective method to realize the resonant response improvement. Theoretical and experimental results are in a well agreement. The resonant frequency can be lifted two times by using triangular cantilever. The fs laser presents its distinguished ability in precise micro-fabrication.

CHAPTER FIVE

CANTILEVER BASED 45° ANGLED FOH

5.1 The principle of the hydrophone

The schematic imaging of a Cantilever based 45° angled FOH is shown in Fig. 5.1. The 45° angled tip was polished precisely from the cleaved endface of a SMF, and the micro-cantilever was fabricated by using fs laser micromachining system to form an open FP cavity on sidewall of the optical fiber. The hydrophone utilized the total internal reflection at 45° angled endface to change the transmission direction of the input light. Sputter coating was applied to do gold coating on the angled endface to improve reflection. The input light would be reflected three times by three interfaces between fused silica and air. Two of the three reflections would cover the gap between a micro-cantilever and the main fiber, and generate interference signal that could be affected by vibration of the micro-cantilever. This sideway looking hydrophone provides a new choice except forward looking detection for endoscopic imaging in vessels.

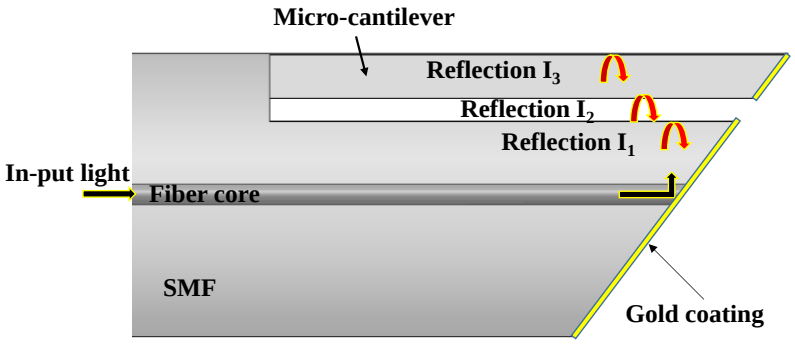

Fig. 5.1. The schematic of side view of a cantilever based 45° angled FOH.

5.2 Sensor fabrication

5.2.1 Sample preparation

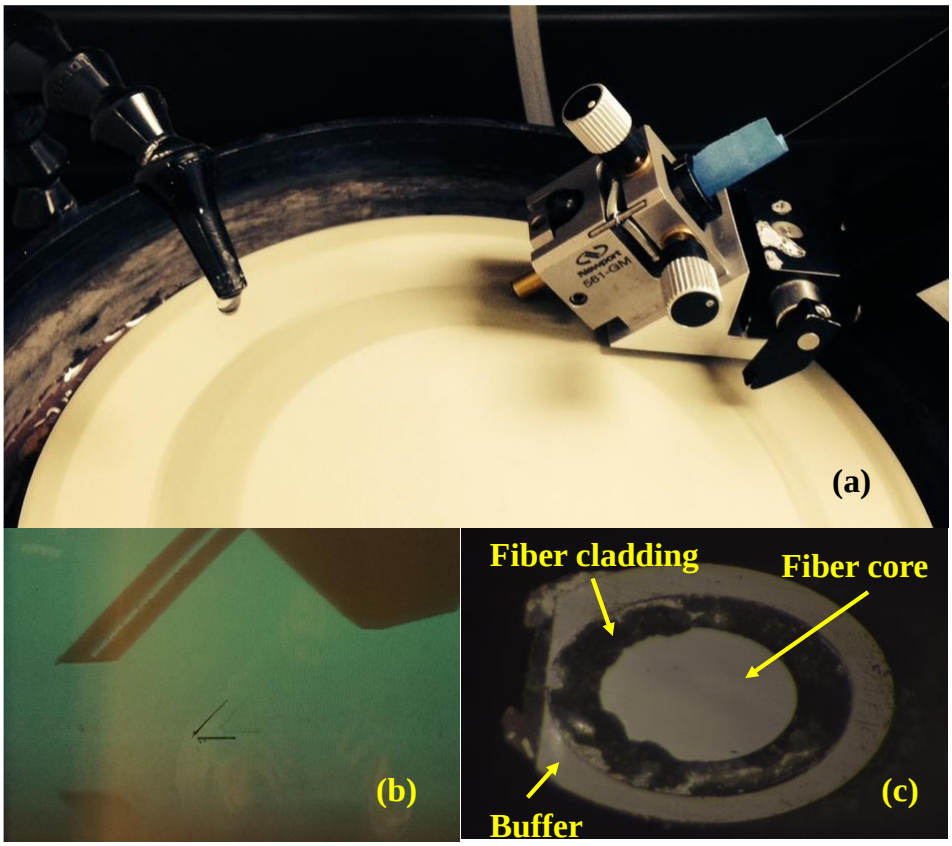

Figure 5.2. (a) Polishing setup for 45° angled fiber, (b) Polishing process in monitoring, (c) Imaging of the polished endface of 45° angled SMF.

The detailed sample preparation process of the 45° angled fiber is shown as follows. A piece of SMF with the length of 1 m was chosen for the experiment. One of the endfaces of the SMF was precisely polished to form a 45° angled end face shown in Fig. 5.3 with using fiber polishing system shown in Fig. 5.2. The fiber was mounted on a home-made fiber holder. The polishing process was performed by a wheel polisher (Ultrapol-1200, Ultra Tec) using diamond lapping films. The rotation speed of polishing plate was set to

be 100 rpm (rounds per minute). Two types of diamond lapping films were used: a lapping film with 3 μm grain size was first used to form an angled fiber endface, and then a lapping film of 0.1 μm grain size was used for fine polishing. Calibration of the polished angles can be carried out by measuring the reflection from the polished fiber endface. The reflection reaches its maximum when a 45° endface is achieved. SEM image of polished 45° angled fiber is shown in Fig. 5.3, which indicates the good quality of the polished angled endface.

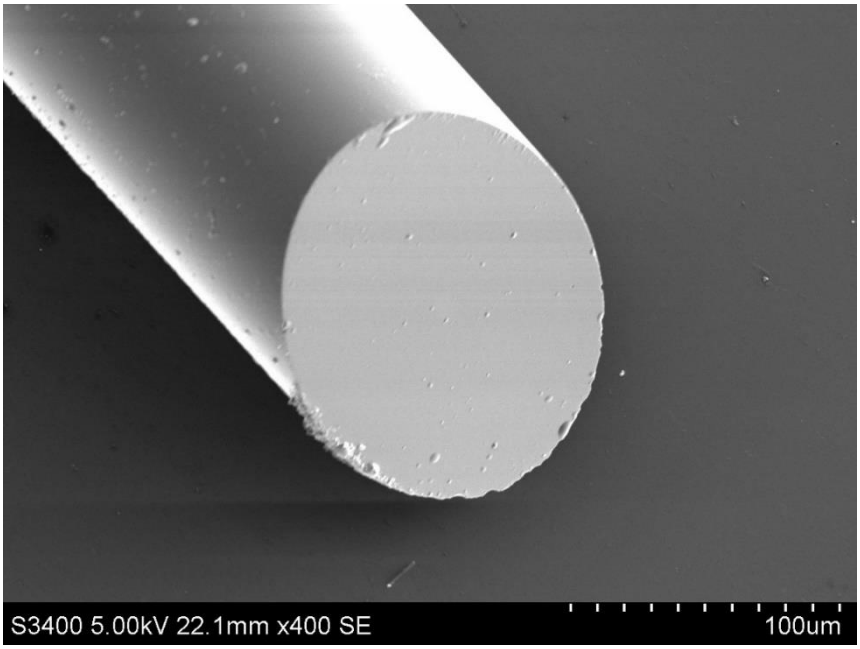

Fig. 5.3. SEM image of polished 45° angled fiber with buffer stripped.

5.2.1 Liquid-assisted laser processing technique

After the angled fiber sample preparation, fs laser was adopted for the fabrication of the micro-cantilever beam on the side surface of the fiber. In 2008, D. Iannuzzi et al. demonstrated a micro-cantilever beam formed on the tip of an SMF using femtosecond

laser irradiation followed by chemical etching (FLICE) technique [89]. In this case, we use another micromachining technique, which is liquid-assisted laser processing technique or fs laser induced water break down (FLIWD) technique, to precisely control the shape of the cantilever beam. Such technique has already been used for the fabrication of microchannel embedded in an SMF and the fabricated device can be used for temperature and refractive index sensing applications [90-91].

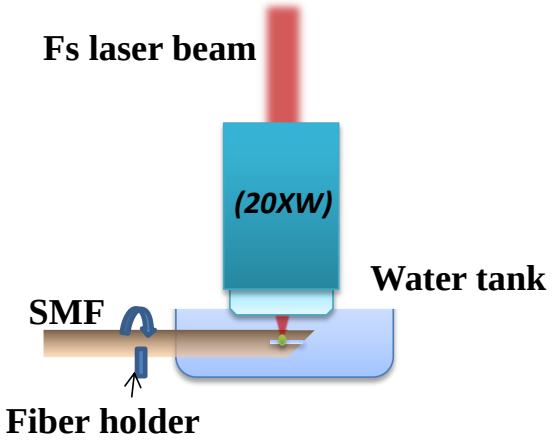

Fig.5.4. Schematic of FLIWD for the fabrication of 3D arbitrary micro-cantilever beam on an SMF with 45° angled endface.

Compared with FLICE technique, FLIWD technique doesn`t have to use any toxic or hazard chemical solutions, such as hydrofluoric acid (HF) or KOH. In addition, the difference of intrinsic etching rates between the germanium-doped core and the pure fused silica cladding [92] can also be ignored. In FLIWD process, the interaction between the laser and the liquid (i.e., DI water) can cause the laser induced water breakdown phenomenon with laser induced bubbles, shockwaves, and a high speed jet. Meanwhile, the water plays a significant role to efficiently remove debris from the ablated regions,

resulting in the formation of micro-cantilever beam with desired shapes. The schematic diagram of FLIWD for the fabrication of 3D micro-cantilever beam on an SMF with 45° angled endface can be found in Fig. 5.4.

5.2.3 Micro-cantilever beam formation

Fig. 5.5 (a) shows the schematic FLIWD micromachining system. The actual laser energy used for fabrication was approximately 0.4 μJ per pulse for low NA lens, which is much higher than the threshold of fused silica. Fig. 5.5 (b) shows the details of FLIWD fabrication process.

The prepared fiber sample with 45° angled endface was cleaned using acetone and clamped in a fiber chuck and then inserted into a fiber holders (Newport 561-FH). The angled fiber was immersed in distilled water during fabrication. The fiber assembly was mounted on a computer-controlled three-axis translation stage (Newport, Inc.) with a resolution of 0.1 μm. The fs laser beam was focused inside the optical fiber through a water immersion objective lens (Olympus UMPlanFL 20x/60x) with a numerical aperture (NA) of 0.4 or 0.9, respectively. The spot size of the focused beam was about 1 μm in fiber for 20x lens, while for 60x lens, the spot size can be reduced down to 1 μm with the pulse energy of 0.4 μJ. The velocities of the stages were set in the range of 50-300 μm/s during fabrication.

A micro-cantilever beam with the dimension of 100×20×20 μm was fabricated using FLIWD method and the microscope image is shown in Fig. 5.6. Obviously, the roughness of the microchannel surface is not smooth enough, which means the optical

insertion loss might be high. If higher NA microscope objective was adopted, the result can be significantly improved. However, high NA lens is hard to operate and easy to be affected by spherical aberration issue.

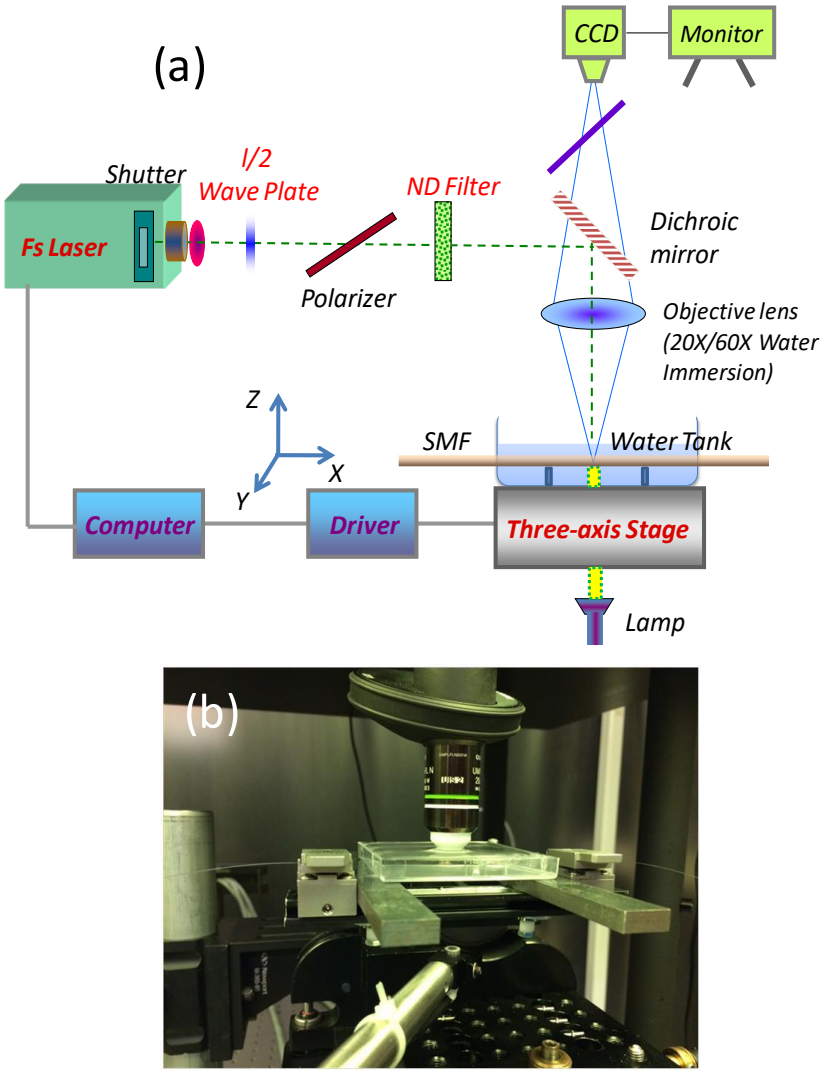

Fig. 5.5. (a) Block diagram of FLIWD for the fabrication of 3D arbitrary micro-cantilever beam on an SMF with 45° angled endface.

(b) Figure of details of FLIWD experiment setup.

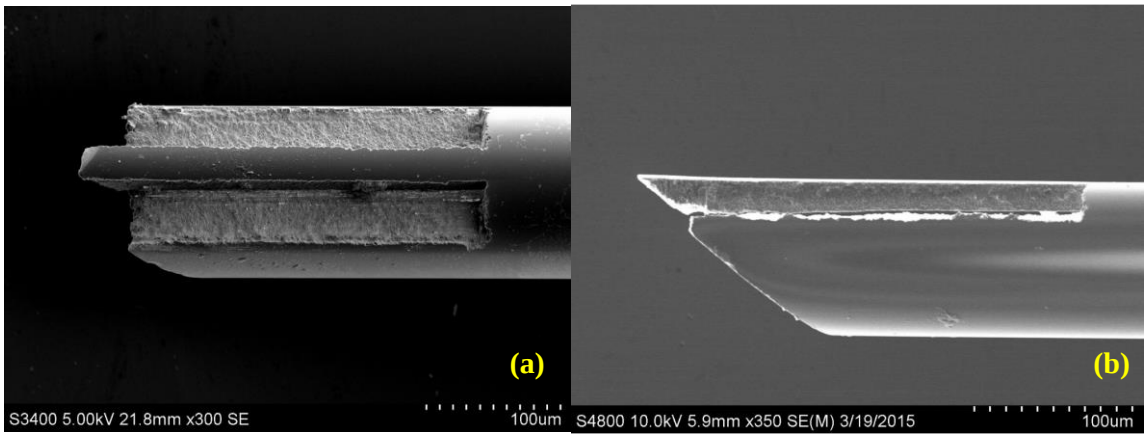

Fig. 5.6. SEM images of (a) top view and (b) side view of the cantilever based hydrophone with 45° angled endface fabricated by FLIDW technique.

After fabrication, the hydrophone would be placed in sputter coating machine in vertical position with angled enface to the top. A thin layer of gold was coated onto the angled endface of the finished structure to improve the reflection on the 45 ° angled endface. It is experimental proved the intensity of signal was improved a lot after coating the angled endface.

5.3 Hydrophone test in water

5.3.1 Predesign of the hydrophones

For co-axial hydrophone, a sensing micro-cantilever was placed on the tip of optical fiber, the dimensions of micro-cantilever could be limited by the size of the diameter of a SMF. When micro-cantilever was set on the sidewall of a SMF, it could be designed much more freely for sensing application.

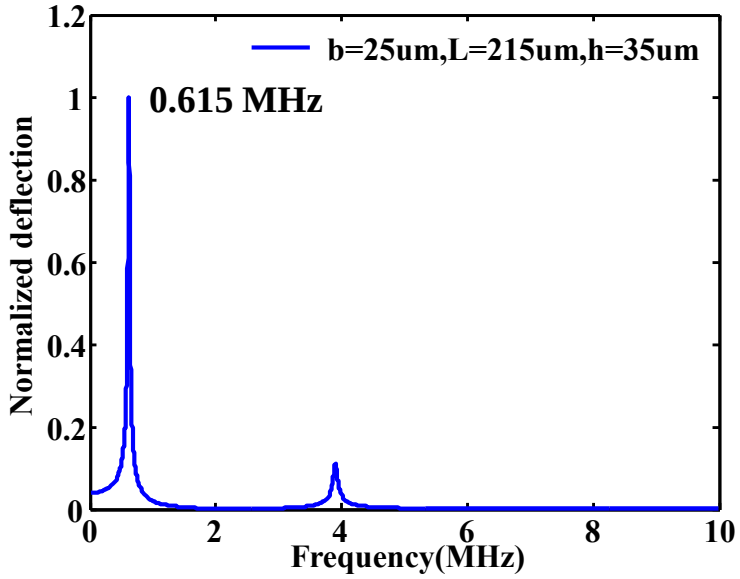

Fig. 5.7. Numerical simulation with MatLAB of frequency response of the hydrophone with size of 215×25×35 μm.

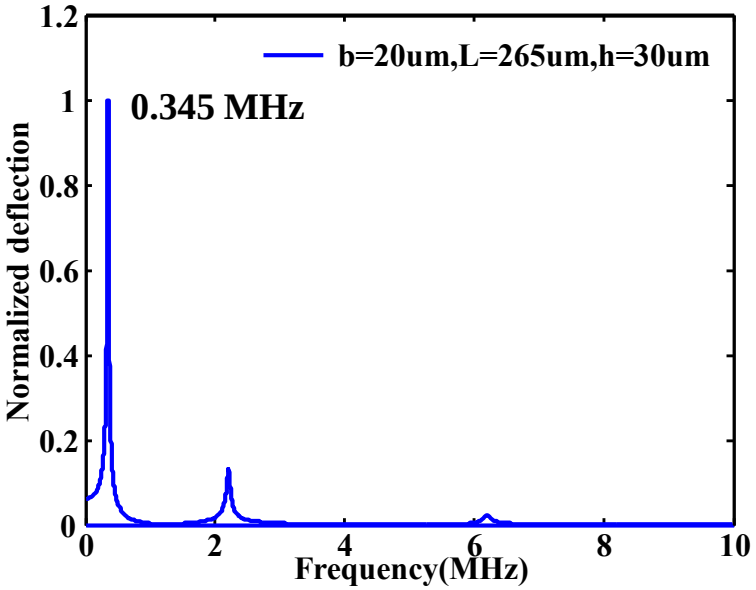

Fig. 5.8. Numerical simulation with MatLAB of frequency response of the hydrophone with size of 265×20×30 μm.

The micro-cantilever at the 45° angled FOH could be simplified to a uniform cross section cantilever. Numerical simulation and predesign could be done using Eq. (2.9). In order to compare frequency responses and sensitivities of two different dimensions of cantilevers based 45° angled FOH, two frequencies are designed below 1MHz. Two frequency responses are shown in Fig. 5.7 and Fig. 5.8 with resonant frequencies of 0.62 MHz and 0.35 MHz. The dimensions of resonant frequency of 0.62 MHz are length of 215 μm, width of 25 μm and thickness of 35 μm. Another one is resonant frequency of 0.35 MHz with size of 265×20×30 μm.

5.3.2 Fabrication of the hydrophones

Fabrication processes are described in details in Section 5.2. Based on simulated two frequency responses of different size cantilevers, the two hydrophones were worked out with help of fs laser micromachining system. Fig. 5.9 shows images of top view and side view of the hydrophone with size of 215×25×35 μm in water in manufacturing process. Another one is shown in Fig. 5.10 in water with size of 265×20×30 μm.

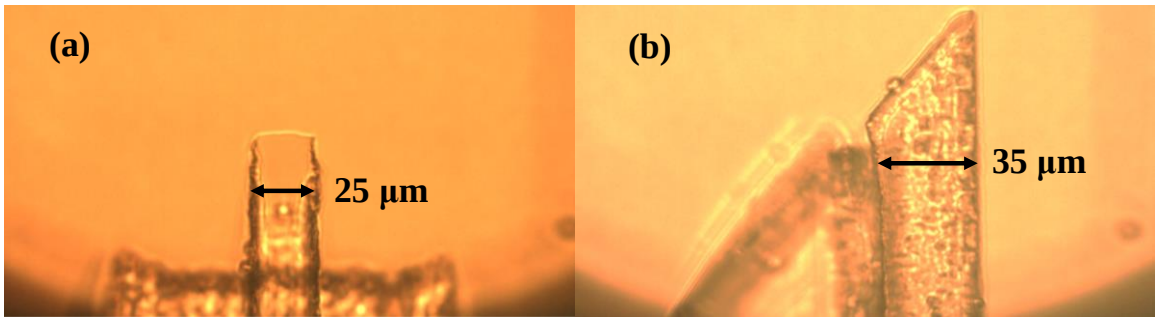

Fig. 5.9. Microscope images of (a) top view and (b) side view of the hydrophone with micro-cantilever size of 215×25×35 μm in manufacturing.

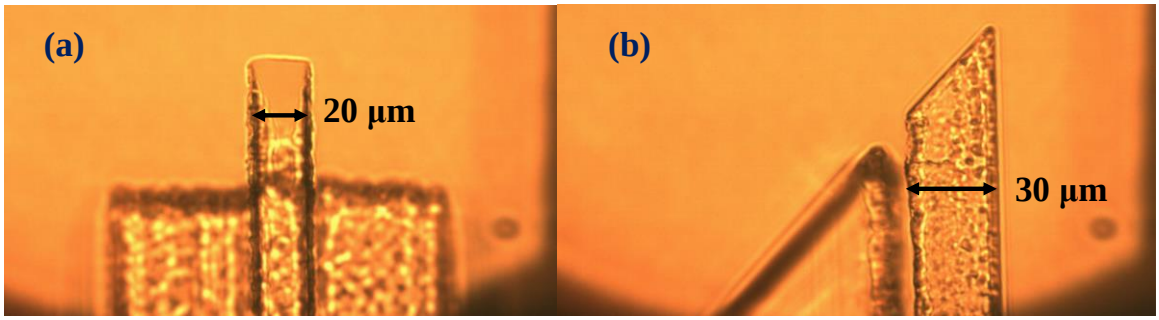

Fig. 5.10. Microscope images of (a) top view and (b) side view of the hydrophone with micro-cantilever size of 265×20×30 µm in manufacturing.

5.3.3 Experimental results and discussion

Micro-cantilever with size of 215×25×35 µm. The reflection spectrum of the hydrophone is demonstrated in Fig. 5.11(a), the operating point is chose at highest response when applied acoustic wave at 0.6 MHz. Fourier transform was applied to the interference spectrum, and then is shown in Fig. 5.11(b). The first peak at 104.4 µm was formed by reflection I_2 and I_3 show in Fig. 5.1, the thickness of the cantilever could be estimated to be 35.5 µm. The second peak at 132 µm was integrated from reflection I_1 and I_3, which cover the gap of 10.4 µm and the micro-cantilever. The dimensions calculated from 5.11(b) verified that fs laser could do precisely fabrication.

The hydrophone was evaluated in range of 0.25-0.7 MHz with step of 0.01 MHz by using OLYMPUS immersion transducer with center frequency of 0.5 MHz. The original frequency response is shown in Fig. 5.12(a). The spectrum is normalized by the frequency response spectrum of the immersion transducer which is shown in the inset of Fig. 5.12(b).

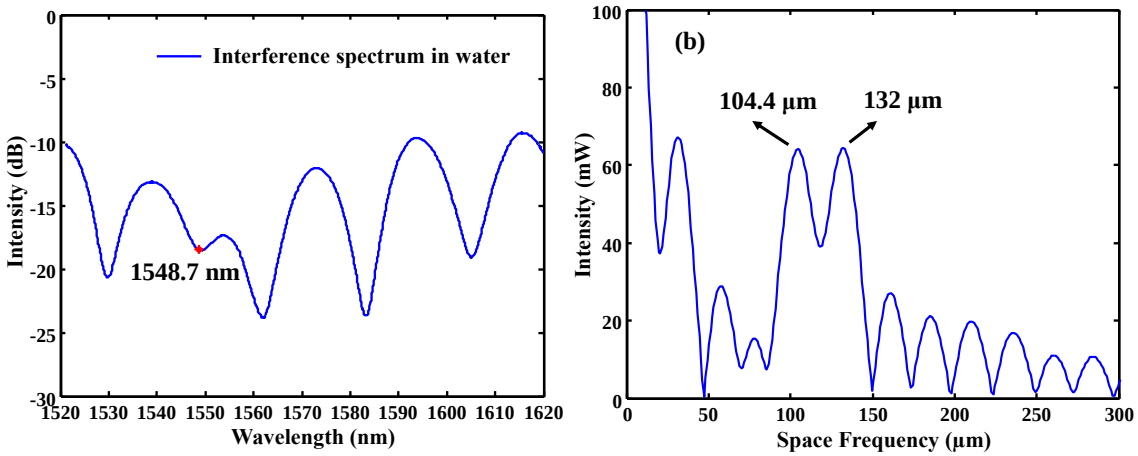

Fig. 5.11. (a) Reflection spectrum of the hydrophone with micro-cantilever size of 215×25×35 µm in water, operating point is chose at 1548.7 nm. (b) FFT result of reflection spectrum.

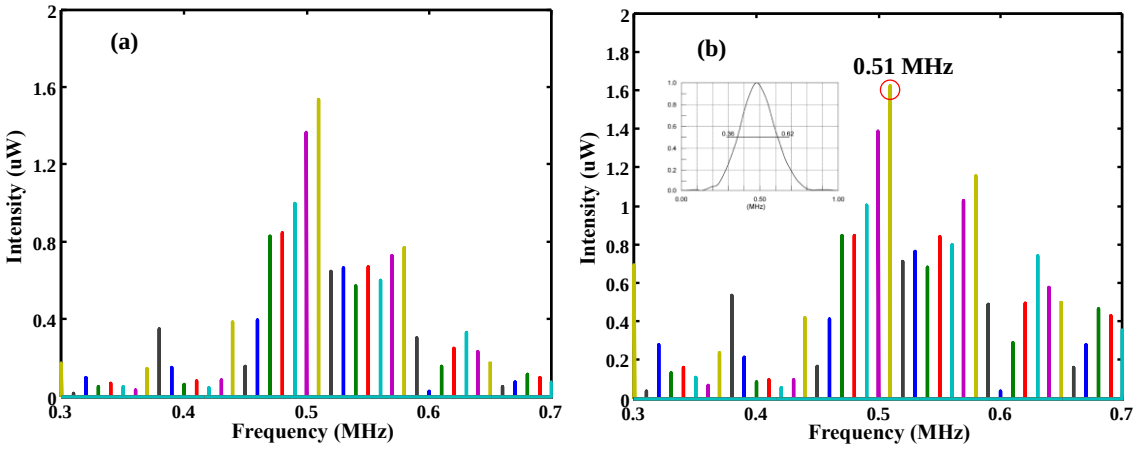

Fig. 5.12. (a) Original frequency response of the hydrophone in the range of 0.3-0.7 MHz. (b) Normalized frequency response of the hydrophone. Inset: frequency response of the OLYMPUS transducer with center frequency of 0.5 MHz.

The normalized spectrum shows that the resonant frequency of the hydrophone is near to 0.51 MHz. We then used a finer step of 0.001MHz to scan through the range of 0.5-

0.6 MHz, the original frequency and normalized frequency are shown in Fig. 5.13(a) and (b). The resonant frequency of the hydrophone is 0.526 MHz, which is near to the simulated result of 0.615 MHz. The output intensity of the hydrophone versus the applied acoustic pressure is plotted in Fig. 5.14, the sensitivity of the cantilever based 45° angled FOH is calculated as 1.56e-5 W/MPa at 526.7 kHz.

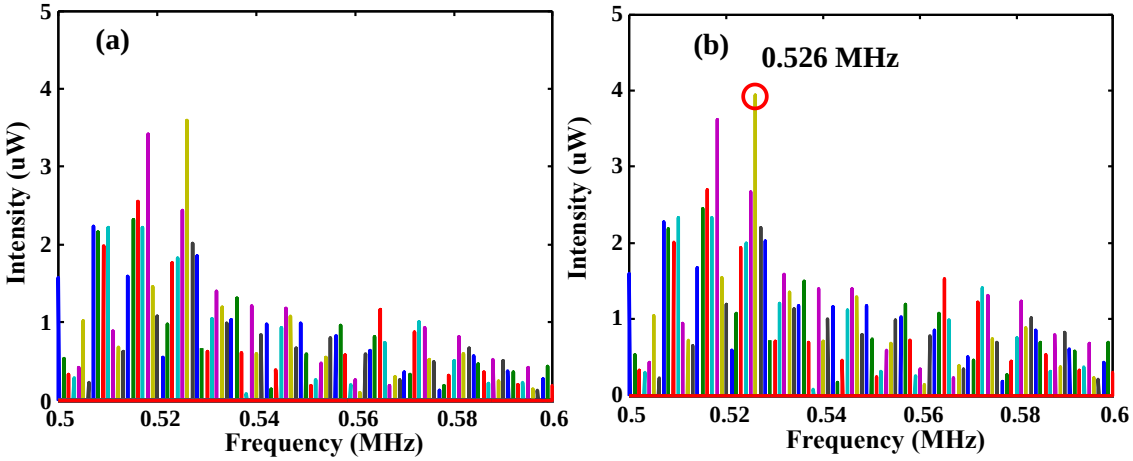

Fig. 5.13. (a) Zoomed-in response spectrum of 5.11(a) and 5.11(b) in range of 0.5-0.6 MHz with step of 0.001MHz.

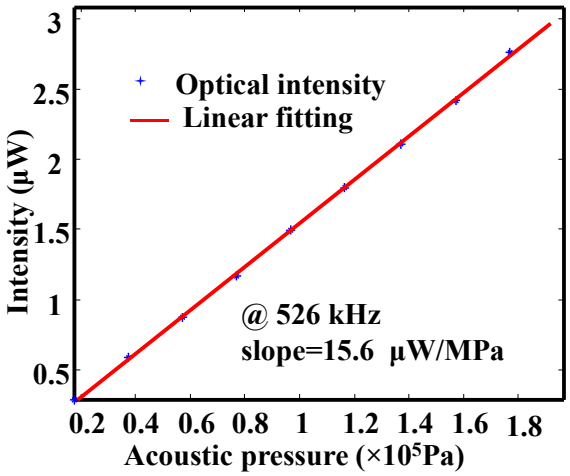

Fig. 5.14. Output intensity of the hydrophone as a function of the applied acoustic sensor.

Micro-cantilever with size of 265×20×30 µm. The interference spectrum of the hydrophone was recorded as shown in Fig. 5.15(a), the operating point was chose at 1541.7 nm when the hydrophone responded highly at acoustic wave frequency of 0.35 MHz. FFT result is shown in Fig 5.15(b). The first peak at 89.6 µm is from interference signal formed by I_2 and I_3, which indicates that thickness of micro-cantilever is 30.5µm. The second peak at 114.2 µm is integrated by reflection I_1 and I_3, the gap between micro-cantilever and main fiber could be calculated is 9.5 µm.

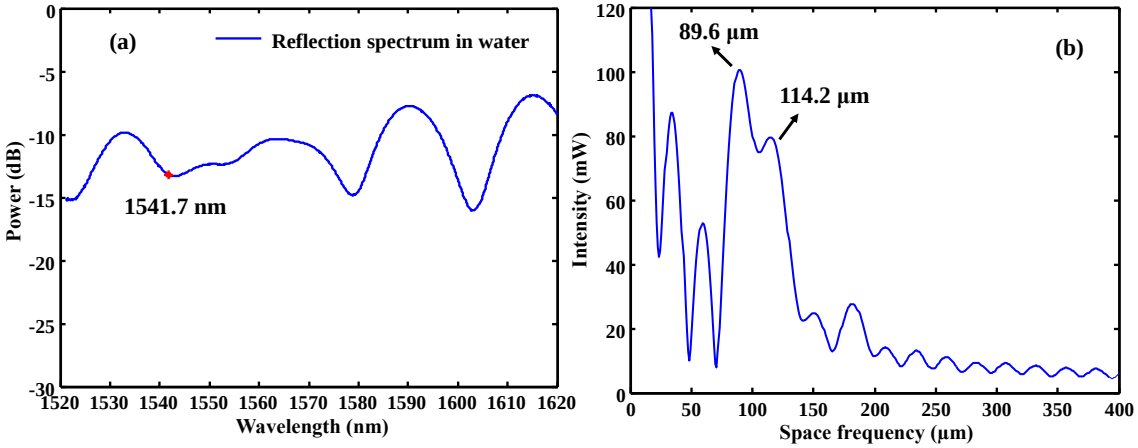

Fig. 5.15. (a) Reflection spectrum of the hydrophone with micro-cantilever size of 265×20×30 µm in water, operating point is chose at 1541.7 nm. (b) FFT result of reflection spectrum.

The resonant frequency of the hydrophone with a 265×20×30 µm micro-cantilever was analyzed to be 0.3451 MHz, so the center frequency of 0.5 MHz immersion transducer was used to test the hydrophone in range of 0.25-0.7 MHz with step of 0.01 MHz. The

original and normalized spectra are shown in Fig. 5.16(a) and (b). The resonant frequency is near to 0.3 MHz.

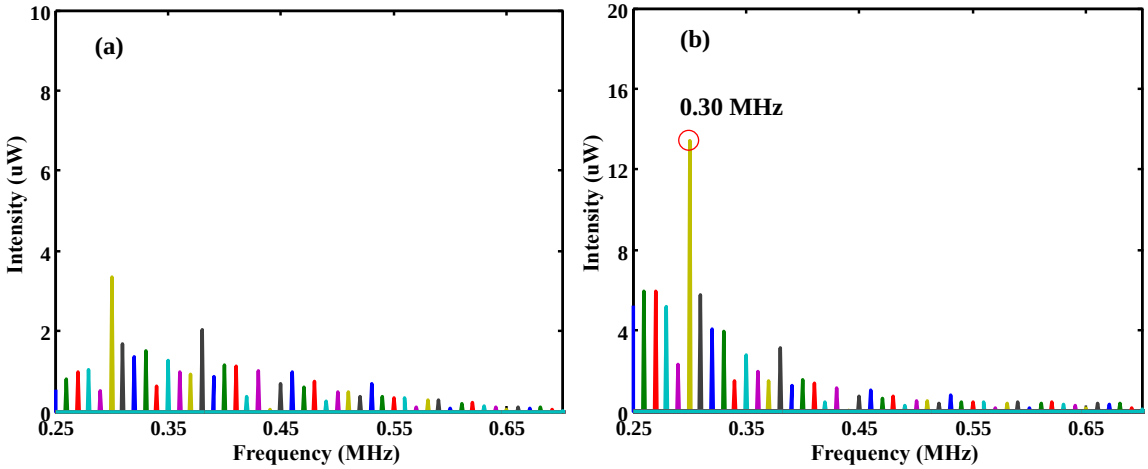

Fig. 5.16. (a) Original frequency response of the hydrophone in the range of 0.25-0.7 MHz. (b) Normalized frequency response of the hydrophone.

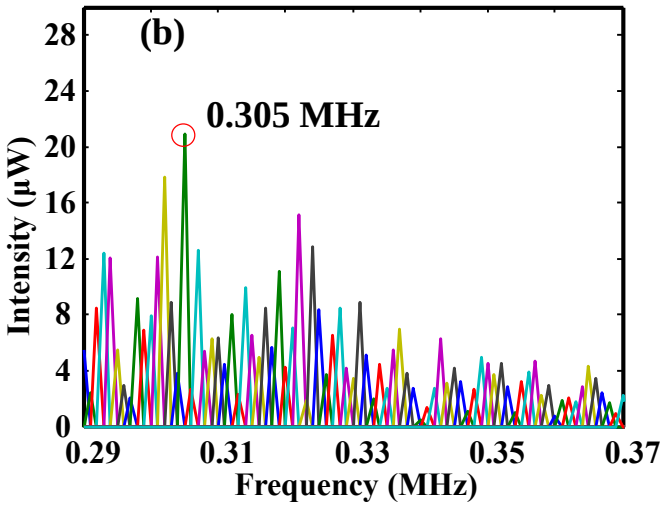

Fig. 5.17. Zoomed in response spectrum of 5.16(b) in the range of 0.29-0.37 MHz.

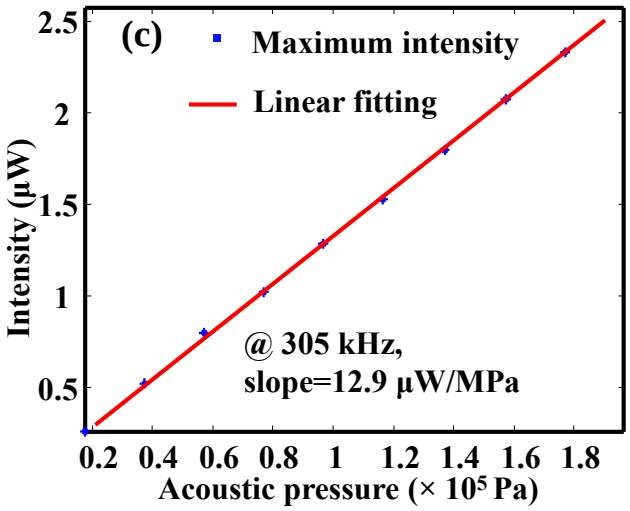

Fig. 5.18. Output intensity of the hydrophone as a function of the applied acoustic sensor.

We used the finer step of 0.001 MHz in range of 0.29-0.37 MHz to find out the resonant frequency of the hydrophone. The final normalized spectrum is shown in Fig.5.17, obviously, the resonant frequency of the hydrophone is at 0.305 MHz, which is in good agreement with the simulated result of 0.3451 MHz. The output intensity of the hydrophone versus the applied acoustic pressure is plotted in Fig. 5.18, the sensitivity of the cantilever based 45° angled FOH is calculated as 1.29e-5 W/MPa at 305 kHz.

5.4 Conclusion

In this chapter, we proposed cantilever based 45° angled FOH for cross-axial sensing applied for endoscopic photoacoustic imaging. Theoretical and experimental investigations have done to realize the concept. The main concept is integrating 45° angled endface and micro-cantilever sensing together. When sensing structure was applied on the sidewall of the hydrophone, the dimensions of the micro-cantilever may have much more

freedoms in design. The hydrophones could easier get down to kilo Hz. The sensitivity of the hydrophone is mainly affected by the length of the micro-cantilever, the tradeoff is the reduction of resonant frequency.

CHAPTER SIX

SUMMARY AND FUTURE WORK

6.1 Briefly summarize the work

Hydrophones are very useful in industrial, military and clinical applications. FOHs have unique advantages of small size, immunity to electromagnetic interferences and capability to be integrated with excitation light source. A miniature FOH could also be used for endoscopic imaging application, especially in photoacoustic imaging in which the target tissue can only be accessed by an endoscopic probe.

The development of hydrophone is described in Chapter 1, especially the various methods of FOHs. For different technologies used in FOHs, EFPI is most common used for acoustic wave detection.

A novel cantilever based FOH was proposed, which comprises an open cavity FPI and a micro-cantilever as sensing element. Acoustic wave applied on the micro-cantilever will make the FPI cavity length changing along with the vibration of the cantilever beam, and then the input single wavelength light would be modulated by acoustic wave, results in the change in optical intensity around the operating point.

Motivated by developing a miniature FOH for endoscopic application in photoacoustic imaging, this dissertation mainly focuses on developing a cantilever based FOH with high level of miniaturization and low unit cost for single use application.

Theoretical and experimental investigations were applied for design, model and test of the cantilever based FOHs. Fs laser micromachining system has been developed for material removal of fused silica in air or in water for the micro-cantilever fabrication.

Following are the specific achievements that can be met with this research:

1. Chapter 2 introduced the principle of EFPI and immersed micro-cantilever beam. The behavior of immersed micro-cantilever under a point load was studied a lot for atomic force microscope. We adopted it to study the frequency response of the uniform cross-section cantilever under the distributed acoustic load for predesign of the sensing part. In order to lift the resonant frequency of the cantilever beam without loss of sensitivity, V-shaped and triangular cantilevers were all investigated using finite element methods with COMSOL. The mechanism of the cantilever based FOH was presented
2. Chapter 3 reported rectangular cantilever based FOH for co-axial sensing in air and in water, and the fabrication process. The cantilever based FOH is a narrow bandwidth, high response around its resonant frequency and high-Q hydrophone. A rectangular cantilever based FOH with size of 75×50×8 μm had highest response near to 0.74 MHz with bandwidth of 0.021 MHz. The sensitivity of the hydrophone was 0.95 μm/MPa, and the limit of detection is about 491.2 Pa at the resonant frequency.
3. Chapter 4 presented V-shaped and triangular cantilever based FOHs for improving resonant frequencies. By changing the shape of sensing structure, the resonant frequency of V-shaped and Triangular cantilever based FOHs would be two times it of the rectangular cantilever based FOH. The thickness and length of the cantilever beams were all similar, V-shaped cantilever based FOH had highest response around 1.36 MHz with relative wide bandwidth of

0.29 MHz. The sensitivity of V-shaped hydrophone was 105 nm/MPa. The triangular cantilever based FOH responded highly at 1.39 MHz with bandwidth of 0.7 MHz. The sensitivity of triangular cantilever based FOH was 582.7 nm/MPa. Those two complex cantilever beam would be affected by fluid much more than rectangular beam that is why these two hydrophones had relative wide bandwidth compared with rectangular cantilever FOH. Due to triangular cantilever was much easier in fabrication and had larger flection area, the triangular cantilever FOH had a little higher sensitivity than the V-shaped cantilever based FOH.

4. Chapter 5 proposed a novel cantilever based 45° angled FOH for cross-axial sensing application. Fs laser micro-machined a micro-cantilever beam paralleled the main optical fiber without restrictions of the diameter of SMF. Experimental results were in good agreement with simulated results. The cantilever based 45° angled FOH with size of 215×25×35 μm had best performance around 0.526 MHz, and the sensitivity was 1.56 W/MPa. The other one with size of 265×20×30 μm had highest response at 0.305 MHz with sensitivity of 1.29 W/MPa.

6.2 Innovations and contributions

Scientific and technical contributions of the research include the following:

1. A novel, open cavity, micro-cantilever based FOH was proposed and realized with help of fs laser precise micromachining system. Experimental

analysis demonstrated dynamic response of the hydrophone, and were in good agreement with theoretical investigation and numerical simulation results.

2. The use of V-shaped and triangular cantilever beams for atomic force microscope inspired the sensing structure design. By changing the shapes of the sensing part of the hydrophone from rectangular cantilever to V-shaped or triangular cantilever, the resonant frequency of the hydrophone could be predesigned and doubled without loss of sensitivity.
3. Cantilever based 45° angled FOH was realized for cross-axial sensing by directing the input light sideways in using total internal reflection on the angled endface. The micro-cantilever as sensing structure had much more space in design. This hydrophone provided an approach in sideways looking detection, which is meaningful for endoscopic application.

6.3 Future work

For clinical photoacoustic imaging application, all optical hydrophone would have many advantages compared with PVDF hydrophone in miniature size and flexibility. In the future, all optical hydrophone must have attractive applications

6.3.1 Improvement of cantilever based FOH

Fs laser could be used for waveguide fabrication in optical fiber [93]. The waveguide fabrication technology could be applied in design of cantilever based FOH, and

made the FOH fabrication easier. Fig. 6.1 shows the schematic of a new cantilever based FOH utilizing waveguide to steer optical axis by 90 ° to the sensing part. The waveguide would direct the input light to the sensing EFPI, the reflected signal will be collected by the waveguide and sent back to the interrogation system through fiber core. It still makes distributed sensing possible by fabricating waveguides and sensing micro-cantilever beams along the optical fiber.

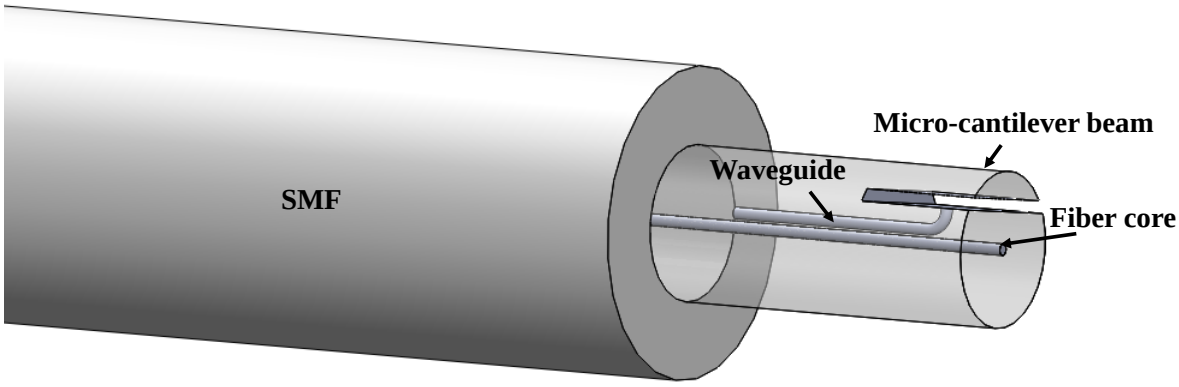

Fig. 6.1. Schematic of cantilever based FOH with waveguide.

6.3.2 Photoacoustic imaging application

As an endoscopic imaging probe, all optical hydrophone could be applied for photoacoustic imaging with help of needle shown in Fig. 6.2. A MMF can be used to transmit the excitation laser light, the cantilever based FOH is used for acoustic wave receiver.

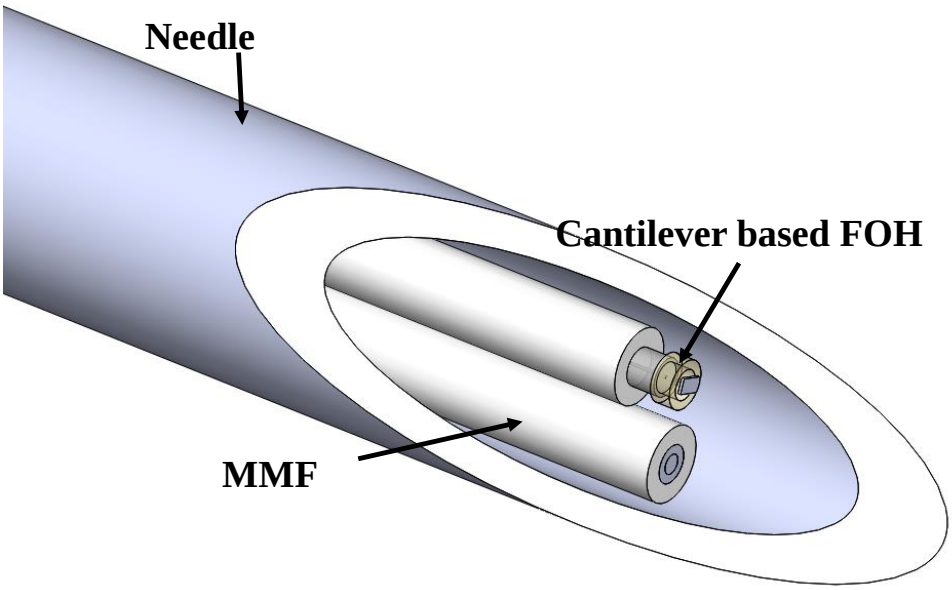

Fig. 6.2. All optical endoscopic imaging probes with help of a needle.

APPENDIX

PUBLICATION LIST

Full List of Journal Publications

2017

[1] **J. Liu**, L. Yuan, J. Lei, W. Zhu, B. Cheng, Y. Song, Q, Zhang, C. Chen, and H. Xiao, "Micro-cantilever based fiber optic hydrophone fabricated by femtosecond laser," ***Optics Letters***, 42(13), 2459-2462, 2017.

[2] L. Yuan, Y. Zhang, **J. Liu**, and H. Xiao, "Ultrafast laser ablation of silica optical fibers for fabrication of diaphragm/cantilever-based acoustic sensors," ***Journal of Laser Applications***, 29 (2), 022206, 2017.

[3] B. Cheng, W. Zhu, **J. Liu**, L. Yuan, and H. Xiao, "3D beam shape estimation based on distributed coaxial cable interferometric sensor," ***Smart Materials and Structures***, 26, 035017, 2017.

2016

[4] L. Yuan, B. Cheng, J. Huang, **J. Liu**, H. Wang, X. Lan, and H. Xiao, "Stress-induced birefringence and fabrication of in-fiber polarization devices by controlled femtosecond laser irradiations," ***Optics Express,*** 24(2), 1062-1071, 2016.

[5] B. Cheng, W. Zhu, L. Hua, **J. Liu**, Y. Li, R. Nygaard, H. Xiao, "Distributed torsion sensor based on cascaded coaxial cable Fabry-Perot interferometers," ***Measurement Science and Technology***, 27(7), 075103, 2016.

[6] Y. Song, L. Hua, J. Lei, Q. Zhang, **J. Liu**, L. Ye, H. Xiao, "An IFPI Temperature Sensor Fabricated in an Unstriped Optical Fiber with Self-Strain-Compensation Function," ***Journal of Sensors***, 2016.

Full List of Conference Presentations:

[1] **J. Liu**, L. Yuan, J. Huang, and H. Xiao, "A cantilever based optical fiber acoustic sensor fabricated by femtosecond laser micromachining," Proceeding of SPIE, Photonics West-LASE, San Francisco, CA, Feb, 2016.

[2] L. Yuan, J. Huang, **J. Liu**, Y. Song, Q. Zhang, J. Lei, and H. Xiao, "Femtosecond laser processing of transparent materials for assembly-free fabrication of photonic microsensors," Proceeding of SPIE-LASE, Photonics West, San Francisco, CA, Feb, 2016.

[3] L. Yuan, B. Cheng, **J. Liu**, J. Huang, and H. Xiao, "All optical fiber polarization controlling devices fabricated by femtosecond laser irradiation," Proceeding of SPIE-LASE, Photonics West, San Francisco, CA, Feb, 2016.

[4] L. Yuan, X. Lan, J. Huang, H. Wang, B. Cheng, **J. Liu**, and H. Xiao, "Miniaturized optical fiber Fabry-Perot interferometer fabricated by femtosecond laser irradiation and selective chemical etching," *Proc. SPIE 8974*, 2014 Advanced Fabrication Technologies for Micro/Nano Optics and Photonics VII, 89741A.

[5] B. Cheng, L. Yuan, X. Fang, X. Lan, **J. Liu**, Y. Ma, H. Shi, Q. Yang, and H. Xiao, "SERS fiber probe fabricated by femtosecond laser with lateral surface silver coating on micro-fiber tips," *Proc. SPIE 8950*, Single Molecule Spectroscopy and Super resolution Imaging VII, 895011 (March 4, 2014).

[6] C. He, **J. Liu**, Z. Liu, B. Wu, "Theoretical Investigation of Propagation of Longitudinal Guided Waves in Cylindrical Pipe Filled with Quiescent or Flowing Fluid: A Foundational Experimental Investigation," Sensor Device Technologies and Applications (SENSORDEVICES***),*** 2010.

BIBLIOGRAPHY

[1] D. Kane, W. Grassi, R. Sturrock, and P. V. Balint, "A brief history of musculoskeletal ultrasound: 'From bats and ships to babies and hips'," Rheumatology (Oxford), vol. 43, pp. 931-3, 2004.

[2] D. Zimmerman, "(introduction)," Paul langevin and the discovery of active sonar or asdic"," Northern Mariner, vol. 12, pp. 39-52, 2002.

[3] K. A. Kaproth-Joslin, R. Nicola, and V. S. Dogra, "The history of US: From bats and boats to the bedside and beyond: RSNA Centennial Article," Radiographics, vol. 35, pp. 960-70, 2015.

[4] S. Davies, C. Edwards, G. Taylor, and S. B. Palmer, "Laser-generated ultrasound: its properties, mechanisms and multifarious applications," Journal of Physics D: Applied Physics, vol. 26, p. 329, 1993.

[5] P. Beard, "Biomedical photoacoustic imaging," Interface Focus, vol. 1, pp. 602-31, 2011.

[6] M. Xu and L. V. Wang, "Photoacoustic imaging in biomedicine," Review of Scientific Instruments, vol. 77, p. 041101, 2006.

[7] S.-L. Chen, L. J. Guo, and X. Wang, "All-optical photoacoustic microscopy," Photoacoustics, vol. 3, pp. 143-150, 2015.

[8] L. V. Wang and J. Yao, "A practical guide to photoacoustic tomography in the life sciences," Nature Methods, vol. 13, pp. 627-38, 2016.

[9] L. F. Brown, "Design considerations for piezoelectric polymer ultrasound transducers," IEEE Transactions on Ultrasonics, Ferroelectrics, and Frequency Control, vol. 47, pp. 1377-1396, 2000.

[10] J. A. Bucaro, H. D. Dardy, and E. F. Carome, "Fiber-optic hydrophone," The Journal of the Acoustical Society of America, vol. 62, pp. 1302-1304, 1977.

[11] G. Wild and S. Hinckley, "Acousto-ultrasonic optical fiber sensors: overview and state-of-the-art," IEEE Sensors Journal, vol. 8, pp. 1184-1193, 2008.

[12] J. G. V. Teixeira, I. T. Leite, S. Silva, and O. Frazão, "Advanced fiber-optic acoustic sensors," Photonic Sensors, vol. 4, pp. 198-208, 2014.

[13] P. Nash, "Review of interferometric optical fibre hydrophone technology," IEE Proceedings-Radar, Sonar and Navigation, vol. 143, pp. 204-209, 1996.

[14] Y. R. García, J. M. Corres, and J. Goicoechea, "Vibration detection using optical fiber sensors," Journal of Sensors, vol. 2010, pp. 1-12, 2010.

[15] S. Foster, S. Goodman, A. Tikhomirov, M. Milnes, and J. V. Velzen, "Recent developments in fiber optic hydrophone technology," 14th International Congress on Sound & Vibration, 2007.

[16] A. A. Oraevsky, E. Z. Zhang, L. V. Wang, and P. C. Beard, "A miniature all-optical photoacoustic imaging probe," vol. 7899, p. 78991F, 2011.

[17] B. T. Cox, E. Z. Zhang, J. G. Laufer, and P. C. Beard, "Fabry Perot polymer film fibre-optic hydrophones and arrays for ultrasound field characterisation," Journal of Physics: Conference Series, vol. 1, pp. 32-37, 2004.

[18] A. A. Oraevsky, L. V. Wang, C. A. Mosse, R. J. Colchester, D. S. Bhachu, E. Z. Zhang, I. Papakonstantinou, and A. E. Desjardins, "Fiber optic ultrasound transducers with carbon/PDMS composite coatings," vol. 8943, p. 89430P, 2014.

[19] P. Beard, F. Perennes, E. Draguioti, and T. Mills, "Optical fiber photoacoustic-photothermal probe," Optics Letters, vol. 23, pp. 1235-1237, 1998.

[20] M. Han, "Diaphragm-based extrinsic Fabry-Perot interferometric optical fiber sensor for acoustic wave detection under high background pressure," Optical Engineering, vol. 44, p. 060506, 2005.

[21] L. H. Chen, C. C. Chan, W. Yuan, S. K. Goh, and J. Sun, "High performance chitosan diaphragm-based fiber-optic acoustic sensor," Sensors and Actuators A: Physical, vol. 163, pp. 42-47, 2010.

[22] J. Deng, H. Xiao, W. Huo, M. Luo, R. May, A. Wang, and Y. Liu, "Optical fiber sensor-based detection of partial discharges in power transformers," Optics & Laser Technology, vol. 33, pp. 305-311, 2001.

[23] E. Cibula and D. Đonlagić, "Miniature fiber-optic pressure sensor with a polymer diaphragm," Applied Optics, vol. 44, pp. 2736-2744, 2005.

[24] S. Ashkenazi, Y. Hou, T. Buma, and M. O'Donnell, "Optoacoustic imaging using thin polymer étalon," Applied Physics Letters, vol. 86, p. 134102, 2005.

[25] Q. Wang and Q. Yu, "Polymer diaphragm based sensitive fiber optic Fabry-Perot acoustic sensor," Chinese Optics Letters, vol. 8, pp. 266-269, 2010.

[26] M. Yang, D. Wang, Y.-J. Rao, Z. Wang, W. Zhang, and F. Li, "Diaphragm-based fiber optic Fabry-Perot hydrophone with hydrostatic pressure compensation," vol. 8924, p. 89241B, 2013.

[27] Y. Cao, W. Jin, H. L. Ho, and J. Ma, "Miniature fiber-tip photoacoustic spectrometer for trace gas detection," Optics Letters, vol. 38, pp. 434-436, 2013.

[28] F. Xu, J. Shi, K. Gong, H. Li, R. Hui, and B. Yu, "Fiber-optic acoustic pressure sensor based on large-area nanolayer silver diaghragm," Optics Letters, vol. 39, pp. 2838-40, 2014.

[29] J. Ma, M. Zhao, X. Huang, H. Bae, Y. Chen, and M. Yu, "Low cost, high performance white-light fiber-optic hydrophone system with a trackable working point," Optics Express, vol. 24, pp. 19008-19, 2016.

[30] Y. Zhang, L. Yuan, X. Lan, A. Kaur, J. Huang, and H. Xiao, "High-temperature fiber-optic Fabry–Perot interferometric pressure sensor fabricated by femtosecond laser," Optics Letters, vol. 38, pp. 4609-4612, 2013.

[31] Y. Liu, P. Lai, C. Ma, X. Xu, A. A. Grabar, and L. V. Wang, "Optical focusing deep inside dynamic scattering media with near-infrared time-reversed ultrasonically encoded (TRUE) light," Nature Communications, vol. 6, p. 5904, 2015.

[32] L. Wang, "Photo acoustic tomography," Scholarpedia, vol. 9, p. 10278, 2014.

[33] J. Staudenraus and W. Eisenmenger, "Fibre-optic probe hydrophone for ultrasonic and shock-wave measurements in water," Ultrasonics, vol. 31, pp. 267-273, 1993.

[34] L. F. Brown, "Design considerations for piezoelectric polymer ultrasound transducers," IEEE Transactions on Ultrasonics, Ferroelectrics, and Frequency Control, vol. 47, pp. 1377-1396, 2000.

[35] H. Gallantree, "Review of transducer applications of polyvinylidene fluoride," IEE Proceedings I-Solid-State and Electron Devices, vol. 130, pp. 219-224, 1983.

[36] A. Seki, K. Iwai, T. Katagiri, and Y. Matsuura, "Forward-viewing photoacoustic imaging probe with bundled ultra-thin hollow optical fibers," Journal of Optics, vol. 18, p. 074015, 2016.

[37] J. Eom, J. G. Shin, S. Park, S. Rim, and B. H. Lee, "An all-fiber-optic combined system of noncontact photoacoustic tomography and optical coherence tomography," Sensors, vol. 16, 2016.

[38] E. Biagi, S. Cerbai, L. Masotti, L. Belsito, A. Roncaglia, G. Masetti, and N. Speciale, "Fiber optic broadband ultrasonic probe for virtual biopsy: technological solutions," Journal of Sensors, vol. 2010, pp. 1-6, 2010.

[39] Y. Miida and Y. Matsuura, "All-optical photoacoustic imaging system using fiber ultrasound probe and hollow optical fiber bundle," Optics Express, vol. 21, pp. 22023-33, 2013.

[40] R. J. Colchester, E. Z. Zhang, C. A. Mosse, P. C. Beard, I. Papakonstantinou, and A. E. Desjardins, "Broadband miniature optical ultrasound probe for high resolution vascular tissue imaging," Biomedical Optics Express, vol. 6, pp. 1502-11, 2015.

[41] B. Yu, D. W. Kim, J. Deng, H. Xiao, and A. Wang, "Fiber Fabry-Perot sensors for detection of partial discharges in power transformers," Applied Optics, vol. 42, pp. 3241-3250, 2003.

[42] A. Arvengas, K. Davitt, and F. Caupin, "Fiber optic probe hydrophone for the study of acoustic cavitation in water," Review of Scientific Instruments, vol. 82, p. 034904, 2011.

[43] W. Spillman and R. Gravel, "Moving fiber-optic hydrophone," Optics Letters, vol. 5, pp. 30-31, 1980.

[44] W. Spillman, "Multimode fiber-optic hydrophone based on a schlieren technique," Applied Optics, vol. 20, pp. 465-470, 1981.

[45] W. B. Spillman and D. H. McMahon, "Schlieren multimode fiber-optic hydrophone," Applied Physics Letters, vol. 37, pp. 145-147, 1980.

[46] D. C. Betz, G. Thursby, B. Culshaw, and W. J. Staszewski, "Acousto-ultrasonic sensing using fiber Bragg gratings," Smart Materials and Structures, vol. 12, p. 122, 2003.

[47] N. Takahashi, A. Hirose, and S. Takahashi, "Underwater acoustic sensor with fiber Bragg grating," Optical Review, vol. 4, pp. 691-694, 1997.

[48] N. Takahashi, K. Yoshimura, S. Takahashi, and K. Imamura, "Development of an optical fiber hydrophone with fiber Bragg grating," Ultrasonics, vol. 38, pp. 581-585, 2000.

[49] J. Shuaiqi, S. Jianye, Z. Nengzhu, H. Lin, and R. Jian, "Detection of ultrasound and photoacoustic imaging with fiber bragg gratings," X-Acoustics: Imaging and Sensing, vol. 1, 2015.

[50] B.-O. Guan, H.-Y. Tam, S.-T. Lau, and H. L. Chan, "Ultrasonic hydrophone based on distributed Bragg reflector fiber laser," IEEE Photonics Technology Letters, vol. 17, pp. 169-171, 2005.

[51] P. Morris, A. Hurrell, A. Shaw, E. Zhang, and P. Beard, "A Fabry-Perot fiber-optic ultrasonic hydrophone for the simultaneous measurement of temperature and acoustic pressure," The Journal of the Acoustical Society of America, vol. 125, pp. 3611-22, 2009.

[52] T. Lim, Y. Zhou, Y. Lin, Y. Yip, and Y. Lam, "Fiber optic acoustic hydrophone with double Mach–Zehnder interferometers for optical path length compensation," Optics Communications, vol. 159, pp. 301-308, 1999.

[53] W. Xia, J. M. Mari, S. J. West, Y. Ginsberg, A. L. David, S. Ourselin, and A. E. Desjardins, "In-plane ultrasonic needle tracking using a fiber-optic hydrophone," Medical Physics, vol. 42, pp. 5983-91, 2015.

[54] P. C. Beard, A. M. Hurrell, and T. N. Mills, "Characterization of a polymer film optical fiber hydrophone for use in the range 1 to 20 MHz: A comparison with PVDF needle and membrane hydrophones," IEEE Transactions on Ultrasonics, Ferroelectrics, and Frequency control, vol. 47, pp. 256-264, 2000.

[55] X. Liu, C. Wang, Y. Shang, C. Wang, W. Zhao, G. Peng, and H. Wang, "Distributed acoustic sensing with Michelson interferometer demodulation," Photonic Sensors, vol. 7, pp. 193-198, 2016.

[56] S. Knudsen and K. Blotekjaer, "An ultrasonic fiber-optic hydrophone incorporating a push-pull transducer in a Sagnac interferometer," Journal of Lightwave Technology, vol. 12, pp. 1696-1700, 1994.

[57] C.-Y. Chao, S. Ashkenazi, S.-W. Huang, M. O'Donnell, and L. J. Guo, "High-frequency ultrasound sensors using polymer microring resonators," IEEE Transactions on Ultrasonics, Ferroelectrics, and Frequency control, vol. 54, 2007.

[58] T. Ling, S. L. Chen, and L. J. Guo, "High-sensitivity and wide-directivity ultrasound detection using high Q polymer microring resonators," Applied Physics Letters, vol. 98, p. 204103, 2011.

[59] A. A. Oraevsky, S.-L. Chen, L. V. Wang, T. Ling, H. W. Baac, and L. J. Guo, "Photoacoustic endoscopy using polymer microring resonators," vol. 7899, p. 78992T, 2011.

[60] H. Bae, X. Zhang, H. Liu, and M. Yu, "Miniature surface-mountable Fabry–Perot pressure sensor constructed with a 45 angled fiber," Optics Letters, vol. 35, pp. 1701-1703, 2010.

[61] J. Yin, T. Liu, J. Jiang, K. Liu, S. Wang, S. Zou, and F. Wu, "Assembly-free-based fiber-optic micro-Michelson interferometer for high temperature sensing," IEEE Photonics Technology Letters, vol. 28, pp. 625-628, 2016.

[62] Y. Yu, W. Zhou, J. Ma, S. Ruan, Y. Zhang, Q. Huang, and X. Chen, "High-temperature sensor based on 45° tilted fiber end fabricated by femtosecond laser," IEEE Photonics Technology Letters, vol. 28, pp. 653-656, 2016.

[63] H. Bae, L. Dunlap, J. Wong, and M. Yu, "Miniature temperature compensated Fabry–Perot pressure sensors created with self-aligned polymer photolithography process," IEEE Sensors Journal, vol. 12, pp. 1566-1573, 2012.

[64] D. Iannuzzi, M. Slaman, J. Rector, H. Schreuders, S. Deladi, and M. Elwenspoek, "A fiber-top cantilever for hydrogen detection," Sensors and Actuators B: Chemical, vol. 121, pp. 706-708, 2007.

[65] J. Li, F. Albri, R. R. Maier, W. Shu, J. Sun, D. P. Hand, and W. N. MacPherson, "A micro-machined optical fiber cantilever as a miniaturized pH sensor," IEEE Sensors Journal, vol. 15, pp. 7221-7228, 2015.

[66] J. Li, F. Albri, J. N. Sun, M. M. Miliar, R. R. J. Maier, D. P. Hand, and W. N. MacPherson, "Fabricating optical fibre-top cantilevers for temperature sensing," Measurement Science and Technology, vol. 25, p. 035206, 2014.

[67] D. Iannuzzi, K. Heeck, M. Slaman, S. de Man, J. H. Rector, H. Schreuders, J. W. Berenschot, V. J. Gadgil, R. G. P. Sanders, M. C. Elwenspoek, and S. Deladi, "Fibre-top cantilevers: design, fabrication and applications," Measurement Science and Technology, vol. 18, pp. 3247-3252, 2007.

[68] A. A. Said, M. Dugan, S. d. Man, and D. Iannuzzi, "Carving fiber-top cantilevers with femtosecond laser micromachining," Journal of Micromechanics and Microengineering, vol. 18, p. 035005, 2008.

[69] L. Yuan, T. Wei, Q. Han, H. Wang, J. Huang, L. Jiang, and H. Xiao, "Fiber inline Michelson interferometer fabricated by a femtosecond laser," Optics Letters, vol. 37, pp. 4489-4491, 2012.

[70] W. Xia, J. M. Mari, S. J. West, Y. Ginsberg, A. L. David, S. Ourselin, and A. E. Desjardins, "In-plane ultrasonic needle tracking using a fiber-optic hydrophone," Medical Physics, vol. 42, pp. 5983-91, 2015.

[71] W. Xia, D. I. Nikitichev, J. M. Mari, S. J. West, R. Pratt, A. L. David, S. Ourselin, P. C. Beard, and A. E. Desjardins, "Performance characteristics of an interventional multispectral photoacoustic imaging system for guiding minimally invasive procedures," Journal of Biomedical Optics, vol. 20, p. 86005, 2015.

[72] J. E. Sader, "Frequency response of cantilever beams immersed in viscous fluids with applications to the atomic force microscope," Journal of Applied Physics, vol. 84, pp. 64-76, 1998.

[73] C. A. Van Eysden and J. E. Sader, "Resonant frequencies of a rectangular cantilever beam immersed in a fluid," Journal of Applied Physics, vol. 100, p. 114916, 2006.

[74] J. E. Sader, "Susceptibility of atomic force microscope cantilevers to lateral forces," Review of Scientific Instruments, vol. 74, pp. 2438-2443, 2003.

[75] J. E. Sader, "Parallel beam approximation for V-shaped atomic force microscope cantilevers," Review of Scientific Instruments, vol. 66, pp. 4583-4587, 1995.

[76] J. P. Cleveland, S. Manne, D. Bocek, and P. K. Hansma, "A nondestructive method for determining the spring constant of cantilevers for scanning force microscopy," Review of Scientific Instruments, vol. 64, pp. 403-405, 1993.

[77] K. Yang, Z. Li, Y. Jing, D. Chen, and T. Ye, "Research on the resonant frequency formula of V-shaped cantilevers," Proceedings of the 2009 4th IEEE International Conference on Nano/Micro Engineered and Molecular Systems, pp. 59-62, 2009.

[78] M. T. Clark and M. R. Paul, "The stochastic dynamics of rectangular and V-shaped atomic force microscope cantilevers in a viscous fluid and near a solid boundary," Journal of Applied Physics, vol. 103, p. 094910, 2008.

[79] R. Hosseini and M. Hamedi, "Study of the resonant frequency of unimorph triangular v-shaped piezoelectric cantilever energy harvester," International Journal of Advanced Design and Manufacturing Technology, vol. 8, 2015.

[80] M. Holmes, N. Parker, and M. Povey, "Temperature dependence of bulk viscosity in water using acoustic spectroscopy," Journal of Physics: Conference Series, p. 012011, 2011.

[81] J. Liu, L. Yuan, J. Lei, W. Zhu, B. Cheng, Q. Zhang, Y. Song, C. Chen, and H. Xiao, "Micro-cantilever-based fiber optic hydrophone fabricated by a femtosecond laser," Optics Letters, vol. 42, pp. 2459-2462, 2017.

[82] L. Yuan, B. Cheng, J. Huang, J. Liu, H. Wang, X. Lan, and H. Xiao, "Stress-induced birefringence and fabrication of in-fiber polarization devices by controlled femtosecond laser irradiations," Optics Express, vol. 24, pp. 1062-1071, 2016.

[83] L. Yuan, J. Huang, X. Lan, H. Wang, L. Jiang, and H. Xiao, "All-in-fiber optofluidic sensor fabricated by femtosecond laser assisted chemical etching," Optics Letters, vol. 39, pp. 2358-2361, 2014.

[84] Z. Chen, L. Yuan, G. Hefferman, and T. Wei, "Ultraweak intrinsic Fabry–Perot cavity array for distributed sensing," Optics Letters, vol. 40, pp. 320-323, 2015.

[85] L. Yuan, Y. Zhang, J. Liu, and H. Xiao, "Ultrafast laser ablation of silica optical fibers for fabrication of diaphragm/cantilever-based acoustic sensors," Journal of Laser Applications, vol. 29, p. 022206, 2017.

[86] L. Yuan, X. Lan, J. Huang, H. Wang, L. Jiang, and H. Xiao, "Comparison of silica and sapphire fiber SERS probes fabricated by a femtosecond laser," IEEE Photonics Technology Letters, vol. 26, pp. 1299-1302, 2014.

[87] L. Yuan, "Femtosecond laser micromachining of advanced fiber optic sensors and devices," Clemson University, 2017.

[88] R. J. Baken and R. F. Orlikoff, Clinical measurement of speech and voice: Cengage Learning, 2000.

[89] A. Said, M. Dugan, S. de Man, and D. Iannuzzi, "Carving fiber-top cantilevers with femtosecond laser micromachining," Journal of Micromechanics and Microengineering, vol. 18, p. 035005, 2008.

[90] K. Zhou, L. Zhang, X. Chen, V. Mezentsev, and I. Bennion, "Microstructures made in optical fiber with femtosecond laser," International Journal of Smart and Nano Materials, vol. 1, pp. 237-248, 2010.

[91] Y. Lai, K. Zhou, L. Zhang, and I. Bennion, "Microchannels in conventional single-mode fibers," Optics Letters, vol. 31, pp. 2559-2561, 2006.

[92] M. Haque, K. K. Lee, S. Ho, L. A. Fernandes, and P. R. Herman, "Chemical-assisted femtosecond laser writing of lab-in-fibers," Lab on a Chip, vol. 14, pp. 3817-3829, 2014.

[93] J. R. Grenier, "Femtosecond laser inscription of optical circuits in the cladding of optical fibers," University of Toronto (Canada), 2016.

VITA

Jie Liu was born in Weinan, Shaanxi Province, China. She completed her B.S. degree in Department of Mechanical Engineering and Automation from Beihang University in 2008. She continued her graduate study in the Department of Mechanical Engineering and Applied Electronics Technology at Beijing University of Technology and received her Master degree in 2011. From July 2011 to July 2012, she worked for NAE (Beijing) Electric Control Technology Ltd. as a mechanical engineer.

In Aug. 2012, Jie went to Missouri University of Science and Technology to pursue her Ph.D. degree. In 2013, Jie started her Ph.D. program in the Department of Electrical and Computer Engineering at Clemson University under the guidance of Dr. Hai Xiao. Her research interest mainly focuses on ultrafast laser micromachining of micro-cantilever based fiber optic hydrophone for sensing applications.

Jie Liu has authored and co-authored 6 high-impact journal papers and 6 conference proceedings during her graduate study. She is an invited member of Phi Kappa Phi, and members of Optical Society of America (OSA), International Society for Optics and Photonics (SPIE), and the Institute of Electrical and Electronics Engineers (IEEE). She served as reviewers for *Ultrasonics*, *Journal of Sensors*, and *Chinese Optics Letters.*